Thermo-economic analysis of a novel integrated structure for liquefied natural gas production using photovoltaic panels

Zahra Alizadeh Afrouzy[1] · Masoud Taghavi[2]

Abstract

As natural gas is not uniformly distributed in different regions of the world, and gas tanks are concentrated in specific geographical areas, gas transfer is a key gas-related industry that greatly contributes to the expansion of this energy carrier's use. For long distances, the use of pipeline transport is uneconomical in practice, and alternative methods should be adopted. From among alternative methods to pipeline transport, natural gas liquefaction is the best and most economic one. A major challenge to the expansion of liquefied natural gas (LNG) use is the energy-consuming process of its production. The liquid gas production process, like other liquefaction processes, consumes considerable amounts of energy. In this paper, a solar energy and natural gas storage method was developed for transfer to far-away regions for demand response by using the DMR compression refrigeration cycle, Kalina power production cycle, and photovoltaic solar panels for the climate of Chabahar coastal city in Southern Iran. The dissipated heat from the DMR compression refrigeration cycle was used as the heat source for the Kalina cycle. The coefficient of performance, specific energy consumption, and exergy yield of the developed integrated structure were 3.201, 0.2293 kWh kg^{-1} LNG, and 42.77%, respectively. The exergy analysis of this integrated structure showed that the largest shares of exergy destruction belonged to solar panels (86.29%) and heat exchangers (6.51%), respectively. The economic analysis of the integrated structure revealed that the payback period, the prime cost of product, and additive value equaled 2.061 years, 0.2500 US$ kg^{-1} LNG, and 0.1156 US$ kg^{-1} LNG, respectively. The results of sensitivity analysis demonstrated that, for the capital cost of 2100 MMUS$ and less, the payback period is < 4 years.

Abbreviations

RTE	Round-trip efficiency
TES	Thermal energy storage
CP	Cryogenic process
CES	Cryogenic energy storage
CASU	Cryogenic air separation units
LACES	Liquid air cryogenic energy storage
BFD	Block flow diagram
PFD	Process flow diagram
LMTD	Logarithmic mean temperature difference
LNG	Liquefied natural gas
NG	Natural gas
DMR	Dual-mixed refrigerant
DSMR	Dual-effect single mixed refrigerant
KSMR	Korea single mixed refrigerant
PV	Photovoltaic
COP	Coefficient of performance
SMR	Single mixed refrigerant
MFC	Mixed-fluid cascade
C_3MR	Propane pre-cooling
MR	Mixed refrigerant
APCI	Air Products and Chemicals, Inc.
AR	Absorption refrigeration
AR-MR1	Absorption refrigeration–mixed refrigerant 1
CO_2	Carbon dioxide
C_p	Specific heat capacity at constant pressure
h	Enthalpy (kJ kg^{-1})
s	Entropy (kJ kg^{-1} °C^{-1})
T	Temperature (°C)
W	Work
ex	Exergy

✉ Zahra Alizadeh Afrouzy
z.afrouzy@yahoo.com

1 Department of Operational Research, Parsa Institute of Higher Education, Babolsar, Iran

2 Department of Mechanical Engineering, Faculty of Noshahr, Mazandaran Branch, Technical and Vocational University (TVU), Noshahr, Iran

Ph	Physical
P	Pressure (kPa)
EES	Engineering equation solver
IEA	International energy agency
Y_F	The system's final yield (kWh kWp^{-1})
E_{AC}	The produced AC energy exiting the inverter (kWh)
P_{PV}	The maximum power produced by the system
Y_A	The amount of DC energy produced by the PV arrays per (kWh)
h	Hot
c	Cold
i	Inlet
o	Outlet
PR	Performance ratio
L	The system's total energy loss
η_{inv}	Inverter efficiency
η_{system}	System efficiency
η_{PV}	Photovoltaic efficiency
ACS	Annualized cost of system
C_{acap}	Annualized capital cost
C_{arep}	Annualized replacement cost
C_{amain}	Annualized maintenance cost
C_{aope}	Annualized operating cost
STC	Standard test conditions
P_{max}	Maximum power
V_{mpp}	Maximum power voltage
I_{mpp}	Maximum power current
V_{oc}	Open circuit voltage
I_{sc}	Short circuit voltage
$\dot{Q}$	Heat rate (kW)
$\dot{W}$	Work rate (kW)
$\dot{Ex}$	Total flow exergy (kW)
W_{sh}	Axial work (kW)
I	Lost exergy (kW)
$\dot{Ex}_{ph}$	Physical exergy (kW)
$\dot{Ex}_{ch}$	Chemical exergy (kW)
$\dot{m}_{in}$	Initial mass flow rate
$\dot{m}$	Mass flow rate (kg.s^{-1})
h_O	Outlet mixture specific enthalpy

Greek letters

$\sum$	Sum
$\int$	Integration
Δ	Difference
η	Isentropic efficiency
λ	Latent heat of vaporization
σ	Entrainment ratio

Components name

HX	Heat exchanger
S	Flash drum
V	Throttling valve

T	Turbine
C	Compressor
P	Pump
MIX	Mixer

Introduction

The choice of a suitable method for gas transfer from among common methods such as pipeline, liquefied natural gas, and liquid hydrocarbons depends on their costs which, in turn, depend on the distance between the origin and the destination of the transfer. For long distances, the use of pipeline transport is uneconomical in practice, and alternative methods should be adopted. From among alternative methods to pipeline transport, liquefaction is the best and most economic one. After being liquefied, natural gas has a much smaller volume of 1:600 and can be transferred over the sea by ships or liquefied natural gas transfer tankers and then be regasified. After being liquefied, natural gas has a much smaller volume of 1:600 and can be transferred over the sea by ships and then be regasified [1]. A major challenge to the use of liquefied natural gas is its energy-consuming process. The liquid gas production process, like other liquefaction processes, consumes considerable amounts of energy. Today, studies on liquefied natural gas industry mostly try to reduce the specific energy consumption in production processes, which reduces the project costs and make the projects more economical. In recent years, extensive research has been conducted to reduce the specific energy consumption in the liquefied natural gas production process.

Vatani et al. [2] performed an energy and exergy analysis of natural gas liquefaction cycles via SMR–Linde (single mixed refrigerant), SMR–APCI (Air Products and Chemicals, Inc.), C$_3$MR–Linde (propane pre-cooled MR), DMR–APCI (dual mixed refrigerant), and MFC–Linde (mixed-fluid cascade) refrigeration cycles. The results of energy analysis showed that liquefaction cycles based on the MFC–Linde refrigeration cycle have the minimum specific energy consumption (0.2545 kWh kg^{-1} LNG), while those based on the SMR–Linde cycle have maximum specific energy consumption (0.3572 kWh kg^{-1} LNG). Vatani et al. [3] performed an advanced economic and exergy analysis of five developed cycles. The results of exergy analysis showed that the liquefaction cycle based on the MFC–Linde refrigeration cycle had the maximum exergy efficiency (51.82%), while the one based on SMR–Linde cycle had the minimum exergy efficiency (40.2%). Ghorbani et al. [4] used the absorption refrigeration cycle as pre-cooling for two integrated natural gas liquefaction structures based on DMR and C$_3$MR refrigeration cycles. The simulation results indicated that by replacing the absorption refrigeration cycle as the pre-cooling in the DMR and C$_3$MR refrigeration cycles,

the specific energy consumption was reduced by 12.6% and 18.4%, respectively. The final liquefied natural gas product cost based on the DMR, C$_3$MR, and AR-MR1 (absorption refrigeration–mixed refrigerant) refrigeration cycles were calculated to be 0.31, 0.28, and 0.26 US$ kg^{-1} LNG, respectively. Ghorbani et al. [5] used the absorption refrigeration cycle as pre-cooling for an integrated natural gas liquefaction structure based on the MFC refrigeration cycle. The simulation results indicated that by replacing the absorption refrigeration cycle as the pre-cooling in the MFC refrigeration cycle, the liquefied natural gas production cost was reduced from 0.305 to 0.237 US$ kg^{-1} LNG [4].

Wang et al. [6] developed two integrated structures for liquefied natural gas production based on DMR and C$_3$MR refrigeration cycles. The final liquefied natural gas product cost based on the DMR and C$_3$MR refrigeration cycles was calculated to be 0.2245 and 0.2242 US$ kg^{-1} LNG, in that order. Moreover, the specific energy consumption of the natural gas liquefaction cycle based on DMR and C$_3$MR refrigeration cycles was calculated to be 2190.2 and 2319.1 MJ/tonne LNG, respectively. Four objective functions of consumption, i.e., compressor shaft work, total investment cost, total annual cost, total compressor purchase, and main low-temperature exchanger cost were analyzed. Qyyum et al. [7] developed two natural gas liquefaction cycles based on DMR and DSMR refrigeration cycles. The specific energy consumption of the natural gas liquefaction cycle based on the DMR and DSMR refrigeration cycles was calculated to be 0.3683 and 0.2840 US$ kg^{-1} LNG, respectively. The exergy efficiency of the natural gas liquefaction cycle based on the DMR and DSMR refrigeration cycles was 28.24% and 36.62%, respectively. Khan et al. [8] developed a new algorithm to optimize the refrigeration cycle of an integrated production system for simultaneous natural gas liquids and liquefied natural gas production. The specific energy consumption of the natural gas liquefaction cycle based on the Korean single mixed refrigerant (KSMR) refrigeration cycle after using the optimization algorithm was reduced from 0.3863 to 0.4241 kWh kg^{-1} LNG. Mehrpooya et al. [9] developed three novel integrated structures for the simultaneous production of natural gas liquids and natural gas liquefaction based on DMR, C3MR, and MFC refrigeration cycles, with the total cycle exergy efficiency of 55%, 56%, and 59%, and the specific energy consumption of 0.391, 0.375, and 0.364 kWh kg^{-1} LNG, respectively. The HYSYS software and the Peng–Robinson equation of state were employed to develop the integrated structure. Shazed et al. [10] used solid oxide fuel cell as a power and heat supply source for the natural gas liquefaction cycle. The simulation results indicated that the energy efficiency and exergy efficiency of the integrated structure were 60% and 55.2%, respectively. The use of fuel cell along with natural gas liquefaction led to a 90% reduction in the produced CO$_2$. Morosuk et al. [11] applied environmental and exergoeconomic analyses on a PRICO process, which is a single mixed refrigerant process. They recommended that the performance of this part be improved since the heat exchanger has the maximum energy dissipation and heavy costs. Khan et al. [12] examined the reduction of specific energy consumption and increasing the liquefied natural gas production when changing the product demand rate under different conditions. The specific energy consumption of the natural gas liquefaction cycle based on the DMR refrigeration cycle after using the optimization algorithm was reduced to 0.3529 kWh kg^{-1} LNG. Husnil et al. [13] proposed an optimal controller structure for the DMR refrigeration process to maintain the compressor's consumption power at the optimal state.

Sun et al. [14] investigated the dynamic performance of a mixed refrigerant system with mixed refrigerant charge and leakage. They created a new model based on process simulation and system specifications. The results showed that light compounds affect pressure because they are mainly in the steam phase, and the effect of heavy compounds is higher on the surface of the tank liquid. The results of this study presented useful information for regulating the mixed refrigerant system and the performance of such as regularization system. Venkatarathnam et al. [15] examined and tested a single-stage JT refrigerator operating with mixtures in this process. The test results showed that a refrigerant that was charged to the system first was changed due to different factors and may lead to an undesirable process performance after some time. Therefore, they found a relationship between the primary charge composition and the charge in the circuit, so that they could find an optimal composition for the primary charge by using the refrigerant mixture in the circuit. Colmenares et al. [16] divided the thermal intervals of the process based on a nonlinear model. The size of the computational model of this method was smaller because it did not need a very precise division of thermal intervals, and it could be solved more quickly. These are the advantages of this method compared to that proposed by Grossmann and Shelton. Vaidyaraman et al. [17] proposed an algorithm for the simultaneous optimization of the choice of an appropriate refrigerant and a refrigeration system. The required data as the input of this algorithm included all the suitable refrigerants and the appropriate intervals for their use. Aghazadeh et al. [18] modeled a novel ejector-cascade refrigeration cycle in engineering equation solver (EES) software, thereby increasing the yield of the multi-stage refrigeration cycles and improving the second law coefficient of performance (COP) and yield of the cascade cycle by about 6.5%. With the advancement of technology and the rise in computers' processing speed in recent years, this method has received the attention of researchers in this field. Nawaz et al. [19] optimized the mixed-fluid cascade LNG process by using

exergy analysis and Coggins stepup approach to reduce compression power. The results indicated that the total exergy losses can be reduced to 34.4%, leading to a 25.5% saving in energy consumption compared to mixed-fluid cascade processes before the optimization. Pereira et al. [20] performed a thermodynamic analysis for liquefaction of natural gas by using the C_3MR refrigeration process. This was done with three levels of propane cooler pressure to predict the specific power consumption of the system with natural gas. The findings showed that increasing the temperature from 30 °C to 50 °C increased the specific power consumption by 0.83. Vikse et al. [21] adopted a non-smooth approach to optimize a DMR process and modeled the polygeneration hybrid solar biomass system. The modeling results indicated that the non-smooth model could reduce the required compression power by 14.4% compared to the preliminary design for the DMR process.

A heavy cost is the main problem associated with the development of photovoltaic (PV) systems. The costs of producing solar cells have been reduced with the progress in technology, but it is still the main challenge. The choice of raw materials for constructing solar panels and cells and the type of technology used in them are key to future planning such that they can directly affect the future of companies and countries. In the first step, the influential factors and criteria in the choice of a specific type of solar cell and panels can determine the efficiency of these cells. But their environmental and economic importance should also be kept in mind. Ebrahimi et al. [22] introduced a novel liquid air cryogenic energy storage system by using the Kalina power cycle, solar parabolic collectors, and phase change materials to examine the integrated structure of simultaneous cooling and electricity production by using the developed solar collectors and regasification of liquefied natural gas.

The results showed that the RTE of electrical energy storage was 45.44% and 57.62%. Gordon et al. [23] proposed a novel strategy for boosting silicon PV efficiency from the regasification of liquefied natural gas. In their proposed method, free cold energy was obtained upon the regasification of liquefied natural gas. The results of this method revealed that an increase of about 80% was obtained in the PV efficiency. Sharadga et al. [24] introduced a novel hybrid system comprising PV panels and thermal solar collectors for electricity production. The dissipated heat of this system was transferred to the Kalina cycle. Based on the results, this hybrid system increased the overall system efficiency by 27%. Ghorbani et al. [25] used the dissipated heat of a hydrogen and oxygen liquefaction cycle for use in the Kalina cycle. The thermal integration of the hydrogen and oxygen liquefaction structure reduced the specific energy consumption and the number of facilities used in the structure. The energy efficiency of the Kalina cycle based on the water–ammonia mixture and the specific energy

consumption of the hydrogen liquefaction cycle equaled 5.46 H_2 kWh kg^{-1} and 14.06%, respectively. Madita et al. [26] developed and optimized a Kalina power cycle based on different refrigerants (water–ammonia, propane–pentane, and methyl amine–water) by using Aspen Plus software and Peng–Robinson equation of state. The optimization results revealed that per 82% by mass of ammonia in the power production cycle based on water–ammonia refrigerant, the maximum yield was achieved. The lower layers of ocean water are used for cooling in the Kalina cycle condenser at a temperature of 6 °C. Naeimi et al. [27] investigated two different methods to heat recovery in the Tehran cement factory. Exergy analysis was used to study the second law of thermodynamics. The exergy efficiencies of the base cycle and first and second scenarios were 47.76%, 73.46%, and 74.86%, respectively. Ghazvini et al. [28] used the invasive weed optimization—SVM method to model and calculate the annual carbon dioxide emission. Various sources of renewable energy, natural gas, coal and oil and GDP of the G8 countries have been used as input in a specified period. Kumar et al. [29] conducted the economic analysis of a coal-fired power plant in the northern part of India. The operating cost, fuel cost, insurance cost, maintenance cost, pumping cost, and net present value have been used to evaluate the power plant.

The liquid gas production process, like other liquefaction processes, consumes considerable amounts of energy. Today, studies on liquefied natural gas industry mostly try to reduce the specific energy consumption in production processes, which reduces the project costs and make the projects more economical. Due to the importance of expanding renewable energies for human life, many researchers have studied these systems in recent years. An attractive source of renewable energy is solar energy which has been greatly expended worldwide owing to its high potential and the diversity of research topics. An exciting technology in this domain is the use of solar panels. In this study, a novel integrated structure for LNG production by using dual mixed refrigerant compression refrigeration cycle, Kalina power production cycle, and PV solar panels is developed. The dissipated heat of the compression refrigeration cycle can be used as a source of energy for the Kalina cycle, thereby increasing COP and reducing energy consumption. Moreover, the use of solar energy as a power production source in regions that receive a suitable amount of solar energy is an important strategy for providing energy in terms of biocompatibility and sustainable development. Figure 1 illustrates the structure of the concerned liquefied natural gas supply chain. The main focus of the developed structure is on the production and economic assessment of liquefied natural gas produced at the source of production.

Fig. 1 The structure of concerned liquefied natural gas supply chain
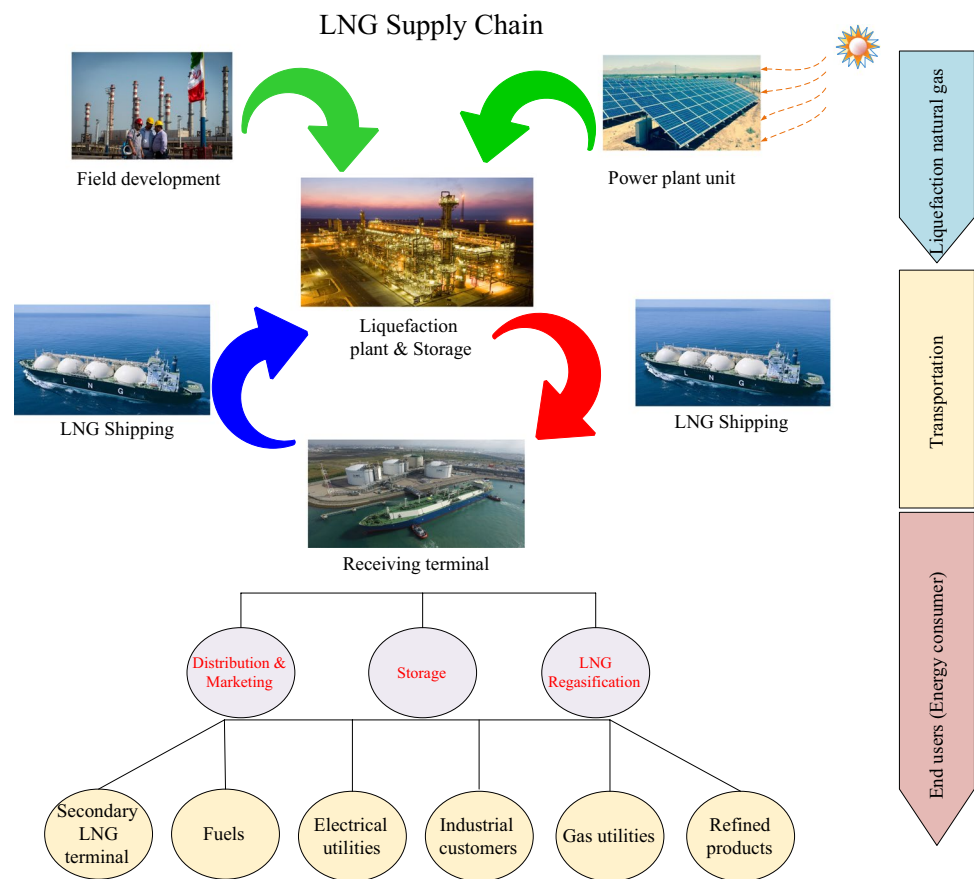
Process description

Low-temperature processes are among the energy-consuming process industries due to the high costs of the equipment and the required energy. A major part of the primary investment and operational costs in these integrated structures belongs to the cooling system costs. Therefore, the optimal design of the cooling system and integrating the processes of the natural gas cold structures greatly reduce the investment costs and consumed energy in a low-temperature process. One optimization method for natural gas liquefaction by using DMR compression refrigeration cycle is the Kalina power production cycle and PV solar panels, developed here based on the climatic conditions of Chabahar coastal city in Southwestern Iran. The minimum temperature difference between the cold and hot composite curves in heat exchangers is assumed as an output parameter. Evidently, the more minimum temperature difference is reduced, the more the driving force for exchanging heat between cold and hot flows is reduced, the more the power consumed by the cycle is reduced, and the more the surface needed for heat exchange is increased. However, since in DMR cycles the minimum temperature difference between cold and hot flows is very small (about 1 to 3 °C), the best option for heat exchangers in these cycles is multi-stream exchangers. In this method,

the integration of the cooling cycle and the processor core is performed in the form of hot and cold composite curves. To simulate the natural gas liquefaction cycle and the Kalina power production cycle, HYSYS and Peng–Robinson equation of state are used. Figure 2 displays the block diagram of the integrated liquefied natural gas production cycle based on the DMR cycle, PV panels, and Kalina power production cycles based on water–ammonia. This integrated structure receives 26.17 MW of power from PV panels and 6771 kmol/h natural gas from the pipeline and produces 6301 kmol/h liquefied natural gas.

Dual mixed refrigerant process

The choice of the best and most suitable natural gas liquefaction technology is a complex and highly sensitive task and requires many design parameters. The selection of the technology for the process and equipment is done based on economical and technical considerations. In this integrated structure, a DMR compression refrigeration cycle is utilized to provide the natural gas liquefaction cycle refrigeration.

Fig. 2 Block diagram of the natural gas liquefaction process by using the DMR compression refrigeration cycle, Kalina power production cycle, and PV solar panels
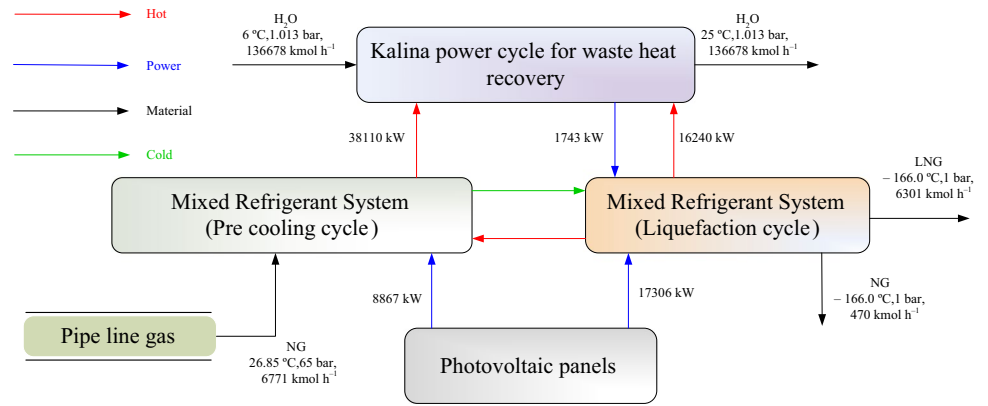
Pre-cooling cycle

Figure 3 illustrates the flow diagram of the natural gas liquefaction cycle by using a DMR cycle, Kalina power production cycle, and PV panels. This cycle is, in fact, the hottest cycle in the process, shown in red. Based on the input flow, this cycle is a combination of 24.82% ethane, 64.16% propane, and 11.03% isobutane. Its main responsibility is to provide the cooling required for the pre-cooling of the input feed and play the role of a cooling source for the coldest cycle by using facilities such as compressors, multi-stream exchangers, throttling valves, and heat exchangers to transfer heat to the Kalina cycle. At 36.85 °C and at a pressure of 17 bars, stream 2 is cooled in the HX1 exchanger to the temperature of 0.08025 °C, exits the exchanger as stream 3, and is divided into two streams, 10 and 4. Stream 10,

which is 60% of the input stream 3, passes the V1 pressure-reducing valve; its pressure is reduced to 7.6 bar and, hence, its temperature is reduced to −3.08 °C. Then, it enters the exchangers, is heated to 32.95 °C, leaves the HX1 exchanger as stream 12, and provides the cooling needed by the HX1 multi-stream exchanger. The rest of stream 3 enters the HX2 multi-stream exchanger to provide a lower level of cooling. After passing this exchanger, it is cooled down to −33.18 °C, enters the V5 throttling valve as stream 5, and its pressure is reduced to 2.8 bars. The pressure reduction is based on the phenomenon of throttling, which leads to a temperature reduction to −36.54 °C (specified by No. 6 in Fig. 3). This cold flow returns to the HX2 exchanger and, after providing the cooling and heating up to −3.08 °C, leaves the exchanger and enters the C2 compressor. After being compressed to the pressure of stream 8 (7.6 bars), streams 8 and 12 enter
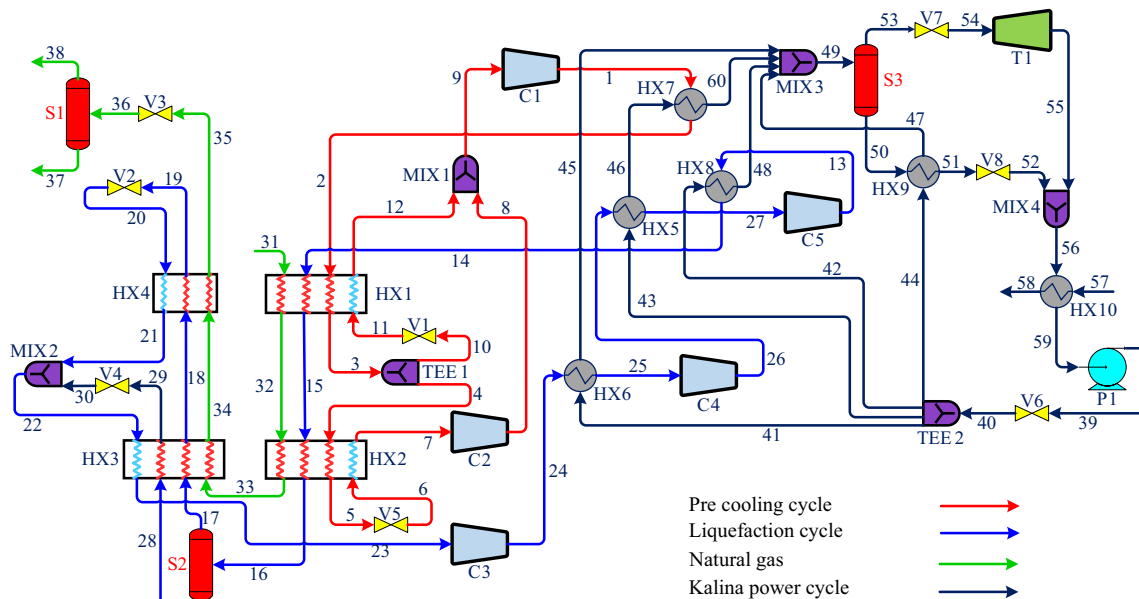
Fig. 3 The flow diagram of the natural gas liquefaction cycle by using heat recycling in the Kalina power production cycle and via PV solar panels

the MIX1. Next, the output flow enters the C1 compressor to increase the pressure to 19.2 bars. The flow exiting the compressor enters the HX7 exchanger, gives 38.11 MW of the dissipated heat at 83.92 °C to the Kalina cycle, and in this way, the main chain of the refrigeration cycle to provide pre-cooling for the integrated structure is completed.

Liquefaction cycle

This DMR cycle (shown in blue in Fig. 3) is in charge of liquefaction and supercooling in the developed integrated structure. This cycle of the DMR comprises a 41.80% methane, 29.9% ethane, 21.30% propane, and 7% nitrogen. Flow 14 at 31.85 °C and a pressure of 48.60 bar enters the HX1 and HX2 multi-stream exchangers, respectively; gives part of its heat to the hotter cycle; and its temperature is reduced by −33.18 °C. The flow exiting the HX2 multi-stream exchanger (under stream 16) enters the S2 flash drum, and the liquid and steam flow exiting from it enter the HX3 multi-stream exchanger. The lighter steam flow exiting from the top of the S2 flash drum enters the HX3 and HX4multi-stream exchangers, respectively, and its temperature is reduced by −128.4 °C and −160.1 °C, respectively. The flow exiting the supercool HX4 exchanger (under Flow 19) passes the V2 throttling valve and reaches a pressure of 3.028 bar. The flow exiting the throttling valve enters the HX4 exchanger again to provide its cooling. Stream 28, which is the output liquid of the S2 flash drum, first enters the HX3 exchanger, is cooled to −4.128 °C, passes the V4 pressure-reducing valve (as stream 29), its pressure is reduced to 3.028 bar, and is mixed with Flow 21 exiting from HX4 exchanger (providing the cooling required by HX4 exchanger). The flow exiting MIX2 (as stream 22) enters the HX3 exchanger to provide its cooling and is heated to −39.61 °C. The heated and low-pressure flow enters the C3 compressor and exits it at a pressure of 20.5 bar. Stream 24 exiting from it enters the HX6 exchanger to provide the heat of the Kalina cycle, and its temperature is reduced by 15 °C. The cooled flow enters the C4 compressor and its pressure is increased by 31.56 bar. The flow exiting the compressor enters the HX5 exchanger for cooling and to provide the heat of the Kalina cycle, and its temperature is reduced by 31 °C. Stream 27 enters the C5 compressor and its pressure is increased by 48.60 bar. The flow exiting the compressor enters the HX8 exchanger, gives 5.146 MW of heat to the Kalina cycle, and in this way, the main chain of the refrigeration cycle to provide final cooling for the integrated structure is completed. More theory and background information on the dual mixed refrigerant is extracted from references [2, 3].

Kalina power production cycle based on water–ammonia refrigerant

The Kalina cycle used low-temperature dissipated heat to produce power. This cycle was proposed by Alexander Kalina and is a thermodynamic process for converting thermal energy to use mechanical power, in which a combination of two fluids with different boiling points is used as the working fluid. Based on the combination of two different fluids, this solution is boiled in higher temperature ranges during distillation, and thus, a larger amount of heat is extracted from the source compared to the pure working fluid. By properly selecting the ratio of the solution fluids, the boiling point of the working solution can be set for the optimization of the heat input temperature. The most common mixture for use in this cycle is water–ammonia. Due to its ability to use all the temperature difference between the source and the thermal well, this cycle is employed in industrial thermal processing, geothermal energy, solar energy, and the application of dissipated heat in integrated structures. This cycle is shown in black in Fig. 3. Table 1 presents the main specifications of the molar composition of the natural gas liquefaction cycle by using DMR compression refrigeration cycle is the Kalina power production cycle and PV solar panels developed based on the climatic conditions of Chabahar coastal city in Southwestern Iran. This cycle of the DMR comprises 83% ammonia and 17% water. Stream 19 enters the TEE2 and is then divided into four parts. Stream 41, which is 16.05% of the input stream 40, passes the HX6 exchanger; its temperature is increased to 78 °C, and it then enters the MIX3 under stream 45. Then, streams 42 and 43 which are 11.14% and 71.08% of the input stream 40, enter HX8 and HX9 exchangers, their temperature is increased to 53.78 and 49 °C, and they enter the MIX3 as streams 46 and 47, respectively. The rest of the flow exiting TEE2, respectively, enters HX5 and HX7 exchangers, its temperature is increased to 78.44 °C, is mixed with the other flows, and enters the S3 flash drum. The gas flow exiting the top of the separator enters the T1 turbine and, by reducing the pressure to 4.5 bars, produces a power of 17.25 kW. The liquid flow exiting the bottom of the flash drum (Stream 50) enters the HX9 exchanger and is used for the pre-heating of the flow entering MIX3. The flow exiting the HX9 exchanger with the molar composition of 32.41% ammonia and 67.59% water enters the V8 throttling valve, its pressure is reduced to 4.5 bars, and it enters the MIX4 mixer as stream 52 with the stream 55 exiting the turbine. The flow exiting mixer MIX4 enters the HX10 condenser and is cooled down to 6.8 °C. To cool down the Kalina cycle, the lower water layers of the Gulf of Oman near Chabahar are used. The cooled flow of water–ammonia enters the P1 pump to increase the pressure to 6.6 bar. Generally, the dissipated heat of the DMR compression refrigeration cycle is used for the Kalina

Table 1 The specifications of the molar compositions of the flows used in the natural gas liquefaction structure

Stream	Nitrogen	Methane	Ethane	Propane	i-Butane	n-Butane	i-Pentane	Ammonia	H_2O
1	0	0	0.248	0.641	0	0.110	0	0	0
13	0.070	0.418	0.299	0.213	0	0	0	0	0
17	0.170	0.655	0.141	0.033	0	0	0	0	0
22	0.070	0.418	0.299	0.213	0	0	0	0	0
28	0.029	0.321	0.363	0.285	0	0	0	0	0
31	0.040	0.875	0.055	0.021	0.005	0.003	0.001	0	0
37	0.015	0.893	0.059	0.022	0.005	0.003	0.001	0	0
38	0.370	0.629	0	0	0	0	0	0	0
39	0	0	0	0	0	0	0	0.830	0.170
49	0	0	0	0	0	0	0	0.821	0.178
50	0	0	0	0	0	0	0	0.324	0.675
53	0	0	0	0	0	0	0	0.963	0.036
56	0	0	0	0	0	0	0	0.830	0.170
57	0	0	0	0	0	0	0	0	1.000

power production cycle, which reduces the specific energy consumption.

Energy analysis

By considering the control volume for each facility used in the development of the integrated structure, with the help of the specific enthalpy value, the energy balance equations can be presented as in Eq. 1 [30]:

$$\sum_{in} \dot{m}_{in} h_{in} - \sum_{out} \dot{m}_{out} h_{out} - \dot{W} + \dot{Q} = 0 \tag{1}$$

In heat exchangers, the energy balance equations can be expressed as follows [31]:

$$\dot{m}_{in,i}(h_{in1,i} - h_{in2,i}) = \dot{m}_{out,i}(h_{out1,i} - h_{out2,i})$$
$$T_{in1,i} = T_{out1,i} + \Delta T_{in,HXi} \tag{2}$$

Note that heat loss is ignored in this equipment. For the energy balance equation of pumps-compressors and turbines, the isentropic yield is used. The following equations are presented in this order [31]:

$$h_{out} = \frac{h_{out}^s - h_{in}}{\eta_s} + h_{in} \tag{3}$$

$$h_{out} = (h_{out}^S - h_{in})\eta_s + h_{in} \tag{4}$$

Moreover, by writing the energy balance and the conservation of mass in the mixer, the following is expressed [31]:

$$\dot{m}_{in,1} h_{in,1} + \dot{m}_{in,2} h_{in,2} = \dot{m}_{out} h_{out} \tag{5}$$

$$\dot{m}_{in,1} + \dot{m}_{in,2} = \dot{m}_{out} \tag{6}$$

By combining Eqs. 5 and 6, the refrigerant's enthalpy at the output of the mixer can be obtained [31]:

$$h_{out} = \frac{\dot{m}_{in,1} h_{in,1} + \dot{m}_{in,2} h_{in,2}}{\dot{m}_{in,1} h_{in,1}} \tag{7}$$

Also, Eqs. 8 and 9 can be used for energy balance and the conservation of mass in the flash drums and separators [31]:

$$\dot{m}_{in} h_{in} = \dot{m}_{out,1} h_{out,1} + \dot{m}_{out,2} h_{out,2} \tag{8}$$

$$\dot{m}_{in} = \dot{m}_{out,1} + + \dot{m}_{out,2} \tag{9}$$

Based on the first law of thermodynamics, the throttling process in throttling valves is a fixed-enthalpy process. Therefore, by taking into account the control volume for these facilities, the following equation is presented [31]:

$$h_{in} = h_{out} \tag{10}$$

PV system simulation

The performance parameters required for the analysis of the performance of the on-grid PV system have been presented by the International Energy Agency (IEA). These parameters are used for a complete analysis of the feasibility study of power plants. The final system yield, denoted by Y_F, denotes the amount of on-grid energy on an annual, monthly, or daily basis. Parameter equals the final amount of AC energy produced by the PV unit to the maximum system power in STC conditions [32].

$$Y_F = \frac{E_{AC}}{P_{PV}} \quad (11)$$

where Y_F refers to the system's final yield per kWh/kWp, E_{AC} is the produced AC energy exiting the inverter per kWh, and P_{PV} resembles the maximum power produced by the system in standard test conditions (STC). The reference yield refers to the nominal efficiency with which the unit is working and is based on the total energy produced by the unit. This nominal efficiency of the unit is determined by the manufacturer in pre-defined STC or standard conditions and can be viewed in the system's datasheet. The reference yield, denoted by Y_R, is mathematically the ratio of the in-plane solar radiation to the array reference irradiance in STC conditions [33]:

$$Y_R = \frac{H_t \ (\text{kWh m}^{-2})}{G_o \ (\text{kW m}^{-2})} \quad (12)$$

The array yield specified by Y_A is in fact equal to the amount of DC energy produced by the PV arrays per kWh to the nominal power of the PV array per kWp in STC conditions [33].

$$Y_A = \frac{E_{DC}}{P_O} \quad (13)$$

The performance ratio (PR) is a fraction of the final system yield to the reference yield [34].

$$PR = Y_F / Y_R \quad (14)$$

The system's total energy loss is calculated using Eq. 15.

$$L = Y_R - Y_F \quad (15)$$

By using Eq. 16, the loss of the array absorber is calculated as the difference between the reference yield and the array yield [35].

$$L_C = Y_R - Y_A \quad (16)$$

Inverter efficiency

The inverter efficiency of a PV system equals the ratio of the inverter's AC power to the DC power produced by the PV array and is calculated based on Eq. 17 [35, 36].

$$\eta_{inv} = \frac{P_{AC}}{P_{DC}} \quad (17)$$

System efficiency

The PV system efficiency is calculated by multiplying the inverter efficiency by the PV module's efficiency and calculated by using Eq. 18 [36].

$$\eta_{system} = \eta_{PV} * \eta_{inv} \quad (18)$$

Exergy analysis

Exergy is the maximum useful work that can be obtained from a specified amount of energy or a flow of materials. To perform exergy analysis, the first law of thermodynamics is employed to calculate the exergy flow in the system and identify the non-optimal components [37].

$$\Delta U = Q - W \quad (19)$$

In addition, by using the second law of thermodynamics, exergy analysis can predict the progress path of reactions, processes, and the amount of loss. In fact, in any actual process, entropy production means exergy destruction in that process.

$$Tds = Q \quad (20)$$

The main aims of exergy analysis are identifying the place and amount of reversibility of different processes in a thermodynamic system, based on which the degree and method of improvement of the system's performance can be specified. The exergy balance for a control volume in the steady-state is presented in Eq. 21 [30].

$$\dot{E}_D = \sum_j \left(1 - \frac{T_0}{T_j}\right) \cdot \dot{Q}_j - \dot{W}_{cv} + \sum_i \dot{Ex}_i - \sum_e \dot{Ex}_e \quad (21)$$

Based on Eq. 22, the exergy rate of the liquid flow $\dot{Ex}$ equals the sum of physical $\dot{Ex}_{ph}$ and chemical $\dot{Ex}_{sh}$ exergy rates [30].

$$\dot{Ex} = \dot{Ex}_{ph} + \dot{Ex}_{ch} \quad (22)$$

Moreover, the physical and chemical exergy rates are given in Eqs. 23 and 24, respectively [30]:

$$\dot{Ex}_{ph} = \sum_i \dot{n}_i \left(\left(\bar{h}_i - \bar{h}_0\right) - T_0\left(\bar{s}_i - \bar{s}_0\right)\right). \quad (23)$$

$$\dot{Ex}_{ch} = \dot{n}\left(\sum_i x_i \overline{ex}_i^{ch,0} + \bar{R} T_0 \sum_i x_i \ln\left(x_i\right)\right) \quad (24)$$

Pump

Pumps are used to increase the pressure of liquids. The pumps used in processes include the input flow, output flow, and the electricity flow related to the electricity consumption. Equation 25 displays the pumps' electricity consumption.

$$\dot{W}_{\mathrm{p}} = \dot{m}\left(h_{\mathrm{o}} - h_{\mathrm{i}}\right) \tag{25}$$

In this equation, $\dot{m}$ is the mass flow velocity; h_{i} and h_{o} are the input and out enthalpy, respectively; and $\dot{W}$ shows the amount of work.

Equation 26 expresses the pumps' exergy balance.

$$I_{\mathrm{p}} = \mathrm{Ex}_{\mathrm{i}} - \mathrm{Ex}_{\mathrm{o}} = \sum (\dot{m}\mathrm{ex})_{\mathrm{i}} + W - \sum (\dot{m}\mathrm{ex})_{\mathrm{o}} \tag{26}$$

where Ex_{i} and Ex_{o} denote input exergy, and output exergy, respectively. Also, Eq. 28 expresses the pumps' exergy efficiency [38].

$$\eta_{\mathrm{ex\text{-}p}} = \frac{\sum (\dot{m}\mathrm{ex})_{\mathrm{i}} - \sum_{\mathrm{i}} (\dot{m}\mathrm{ex})_{\mathrm{o}}}{W} \tag{27}$$

Compressor

Compressors can be used to reduce the volume and, hence, increase the pressure of gases. The input flow, output flow, and the electrical current related to the electricity consumption are the compressor parameters used in processes. Equation 28 shows the compressor's electricity consumption.

$$\dot{W}_{\mathrm{c}} = C_{\mathrm{p}}\left(T_{\mathrm{o}} - T_{\mathrm{i}}\right) \tag{28}$$

where T_{i} is the input temperature, and T_{o} denotes the output temperature. Equation 29 shows the compressor's exergy balance.

$$I_{\mathrm{c}} = \mathrm{Ex}_{\mathrm{i}} - \mathrm{Ex}_{\mathrm{o}} = \sum (\dot{m}\mathrm{ex})_{\mathrm{i}} + W - \sum (\dot{m}\mathrm{ex})_{\mathrm{o}} \tag{29}$$

where Ex_{i} and Ex_{o} denote input exergy, and output exergy, respectively. Equation 30 indicates the compressor's exergy efficiency [30].

$$\eta_{\mathrm{ex\text{-}c}} = \frac{\sum (\dot{m}\mathrm{ex})_{\mathrm{i}} - \sum_{\mathrm{i}} (\dot{m}\mathrm{ex})_{\mathrm{o}}}{W} \tag{30}$$

Turbine

Turbines are rotary mechanical devices that receive energy from the fluid flow and convert this energy into useful work and power. Equation 31 demonstrates the turbines' electricity consumption.

$$\dot{W}_{\mathrm{t}} = \dot{m}\left(h_{\mathrm{i}} - h_{\mathrm{o}}\right) \tag{31}$$

Equation 32 indicates the turbines' exergy destruction.

$$\mathrm{Ex}_{\mathrm{D,T}} = \mathrm{Ex}_{\mathrm{i}} - \mathrm{Ex}_{\mathrm{o}} = \sum (\dot{m}\mathrm{ex})_{\mathrm{i}} - W - \sum_{\mathrm{i}} (\dot{m}\mathrm{ex})_{\mathrm{o}} \tag{32}$$

Equation 33 indicates the turbines' exergy efficiency [30].

$$\eta_{\mathrm{ex\text{-}t}} = \frac{W}{\sum (\dot{m}ex)_{\mathrm{i}} - \sum_{\mathrm{i}} (\dot{m}ex)_{\mathrm{o}}} \tag{33}$$

Heat exchanger

Heat exchangers are important facilities in the process. Equation 34 shows the heat exchanger's exergy destruction.

$$\mathrm{Ex}_{\mathrm{D,HX}} = \mathrm{Ex}_{\mathrm{i}} - \mathrm{Ex}_{\mathrm{o}} = \sum (\dot{m}\mathrm{ex})_{\mathrm{i}} - \sum_{\mathrm{i}} (\dot{m}\mathrm{ex})_{\mathrm{o}} \tag{34}$$

Equation 35 shows the exergy destruction for a multi-stream heat exchanger [30].

$$\mathrm{Ex}_{\mathrm{D,HX}} = 1 - \left\{ \left[\frac{\sum_1^n (\dot{m}\Delta\mathrm{ex})}{\sum_1^n (\dot{m}\Delta\mathrm{eh})} \right]_{\mathrm{h}} - \left[\frac{\sum_1^n (\dot{m}\Delta\mathrm{ex})}{\sum_1^n (\dot{m}\Delta\mathrm{eh})} \right]_{\mathrm{c}} \right\} \tag{35}$$

Throttling valve

Pressure-reducing valves have no heat transfer to the environment and are, in fact, isenthalpic equipment. Equations 36–38 indicate the efficiency and exergy destruction of the pressure-reducing valve [4].

$$h_{\mathrm{i}} = h_{\mathrm{e}} \tag{36}$$

$$\mathrm{Ex}_{\mathrm{D,HX}} = \mathrm{Ex}_{\mathrm{i}} - \mathrm{Ex}_{\mathrm{o}} = \sum (\dot{m} \cdot \mathrm{ex})_{\mathrm{i}} - \sum (\dot{m} \cdot \mathrm{ex})_{\mathrm{o}} \tag{37}$$

$$\eta_{\mathrm{ex}} = \frac{e_{\mathrm{o}}^{\Delta T} - e_{\mathrm{i}}^{\Delta T}}{e_{\mathrm{i}}^{\Delta p} - e_{\mathrm{o}}^{\Delta p}}$$
$$e^{\Delta T} = \int_T^{T_0} \frac{T - T_0}{T} d\mathrm{h}, \quad e^{\mathrm{Ph}} = e^{\Delta T} + e^{\Delta T} \tag{38}$$

Economic analysis

The method adopted for the economic assessment of the natural gas liquefaction hybrid unit by using heat recycling in the Kalina power production cycle and solar panels is the annualized cost of system (ACS) method. In this procedure, all the costs of a system in its predicted technical lifetime are calculated. These costs include the annualized capital price (C_{acap}), annualized replacement price (C_{arep}), annualized maintenance price (C_{amain}), and annualized operating price (C_{aope}). Since the project's useful life is assumed to be 20 years, the C_{arep} is ignored [4]. For the economic assessment of the facilities of integrated structures, the equations given in references have been used. Many of these equations

for previous years are updated by using Marshal and Swift cost indices [39].

$$\text{Cost}_{\text{reference year}} = \text{Cost}_{\text{original year}} \frac{\text{Cost index}_{\text{reference cost year}}}{\text{Cost index}_{\text{original cost year}}} \tag{39}$$

The fixed capital investment and other outlays be considered to calculate the price of equipment. The fixed capital investment includes direct cost and indirect cost. Equations 40–44 have been used to calculate economic assessment [39, 40]:

$$\begin{aligned}
C_{\text{Cap}} = & \sum_k \left(C_k^{\text{MHX}} \right) + \sum \left(C_k^{\text{Com}} \right) + \sum \left(C_k^{\text{Con}} \right) + \sum \left(C_k^{\text{Pump}} \right) + \sum_k \left(C_k^{\text{GHX}} \right) \\
& + \sum_k \left(C_k^{\text{FD}} \right) + \sum_k \sum_m \left(C_m^{\text{PV}} \right) + \left(C_m^{\text{Battery}} \right) + \left(C_m^{\text{Inverter}} \right) + \left(C_m^{\text{Diesel}} \right) \\
& + \sum_k \sum_m \left(C_m^{\text{Onsite price}} \right) + \sum_k \sum_m \left(C_m^{\text{Offsite price}} \right) + \sum_k \sum_m \left(C_m^{\text{Indirect price}} \right) \\
& + \sum_k \sum_m \left(C_m^{\text{Other outlys}} \right)
\end{aligned} \tag{40}$$

$$\begin{aligned}
\sum_k \sum_m \left(C_m^{\text{Onsite price}} \right) = & \sum_k \left(C_m^{\text{Purchased equipment installation}} \right) + \sum_k \left(C_m^{\text{Piping}} \right) + \sum_k \left(C_m^{\text{Instrumentation and control}} \right) \\
& + \sum_k \left(C_m^{\text{Electrical equipment and material}} \right)
\end{aligned} \tag{41}$$

$$\sum_k \sum_m \left(C_m^{\text{Offsite price}} \right) = \sum_k \left(C_m^{\text{Engineering and supervision}} \right) + \sum_k \left(C_m^{\text{Construction cost}} \right) + \sum_k \left(C_m^{\text{Icontingencies}} \right) \tag{42}$$

$$\sum_k \sum_m \left(C_m^{\text{Other outlys}} \right) = \sum_k \left(C_m^{\text{Working Capital}} \right) + \sum_k \left(C_m^{\text{Sturtup}} \right) \tag{43}$$

$$\begin{aligned}
C_{\text{Cap}} = & \sum_k \sum_m \left(C_{\text{cap}} \cdot \text{CRF}(i, Y_{\text{project}}) \right)_m + \sum_k \sum_m \left(C_{\text{rep}} \cdot \text{SSF}(i, Y_{\text{project}}) \right)_m + \sum_k \sum_m \left(C_{\text{amain}} \right)_m \\
& + \sum_k \sum_m \left(C_{aope} \right)_m
\end{aligned} \tag{44}$$

Results and discussion

In this paper, a liquefied natural gas production integrated structure based on the DMR cycle is developed. The heat dissipated from the hybrid unit is used as the input heat to the Kalina cycle based on the water–ammonia mixture. The use of dissipated heat for providing power reduces the specific energy consumption and increases cycle yield. To provide the power of the compressors of this natural gas liquefaction integrated structure, PV panels compatible with the

Chabahar climatic conditions in Iran are applied. Herein, to simulate the PV system in Chabahar (60°38' east longitude, 25°17' north latitude, and 7 m height above the sea level), the PVsyst 6.8.1 software is used. Moreover, the depth of the Gulf of Oman around Chabahar is about 3398 m.

Energy analysis results

Table 2 presents the operational specifications of the flows, including temperature, pressure, and molar flow rate for simulation in the HYSYS software. The Peng–Robinson state equation is selected to simulate the integrated structure in HYSYS.

In recent years, energy consumption optimization has been a major concern in all energy-consuming industries. For the past decades, with a reduction in fossil fuel sources, the energy crisis has become a major global problem. This problem, besides the increase in environmental pollutions resulting from the consumption of fossil fuels, has made energy saving an important strategy in all industries. Over time, various solutions have been put forward for energy saving, including the re-use of energy dissipated in units. In this regard, various methods have been proposed for the re-use of dissipated energies, known as thermal energy recycling.

Table 2 Operational specifications of the streams applied in the hybrid system

Stream	Temperature/°C	Pressure/kPa	Molar entropy/ kJ kmol^{-1} °C^{-1}	Molar entropy/ kJ kmol^{-1}	Molar flow/kmol h^{-1}
1	83.92	1920.00	−98,798.83	159.77	8265.04
2	36.85	1920.00	−115,398.47	108.38	8265.04
3	−0.08	1920.00	−119,821.70	93.22	8265.04
4	−0.08	1920.00	−119,821.70	93.22	3306.02
5	−33.18	1920.00	−123,198.08	80.06	3306.02
6	−36.54	280.00	−123,198.08	80.55	3306.02
7	−3.08	280.00	−103,889.99	157.59	3306.02
8	44.12	760.00	−100,959.13	159.94	3306.02
9	37.44	760.00	−101,488.57	158.25	8265.04
11	−3.08	760.00	−119,821.70	93.56	4959.02
12	32.95	760.00	−101,841.53	157.10	4959.02
13	62.24	4860.00	−78,765.88	160.10	9052.62
14	31.85	4860.00	−80,812.22	153.70	9052.62
15	−0.08	4860.00	−85,637.15	136.90	9052.62
16	−33.18	4860.00	−90,048.96	119.72	9052.62
17	−33.18	4860.00	−68,371.91	141.16	2610.82
20	−166.58	302.79	−80,065.32	77.56	2610.82
21	−132.38	302.79	−73,571.76	130.18	2610.82
22	−132.87	302.79	−96,518.25	91.85	9052.62
23	−39.61	302.79	−81,928.97	169.48	9052.62
24	79.59	2050.00	−76,653.57	172.56	9052.62
25	15.00	2050.00	−80,247.91	161.31	9052.62
28	−33.18	4860.00	−98,834.52	111.04	6441.80
29	−128.45	4860.00	−105,818.30	74.45	6441.80
30	−133.95	302.79	−105,818.30	76.24	6441.80
31	26.85	6500.00	−74,897.43	148.77	6771.36
32	−0.08	6500.00	−76,215.87	144.17	6771.36
33	−33.18	6500.00	−78,096.15	136.81	6771.36
34	−128.45	6500.00	−87,151.35	90.31	6771.36
35	−160.15	6500.00	−88,951.75	76.28	6771.36
36	−166.04	100.00	−88,951.75	78.51	6771.36
37	−166.04	100.00	−91,610.50	73.69	6301.41
40	6.84	660.00	−107,043.64	72.25	9092.00
41	6.84	660.00	−107,043.64	72.25	1459.51
44	6.84	660.00	−107,043.64	72.25	157.00
46	18.92	660.00	−105,898.00	76.24	6462.67
47	49.00	650.00	−89,510.58	130.84	157.00
48	53.78	660.00	−88,753.46	133.09	1012.83
51	55.68	630.00	−214,982.20	71.27	1894.60
52	55.71	450.00	−214,982.20	71.28	1894.60
55	61.65	450.00	−52,308.08	161.98	7197.40
56	61.03	450.00	−86,206.29	143.08	9092.00
57	6.00	101.30	−286,986.06	50.63	136,678.02
60	78.44	660.00	−84,668.89	145.12	6462.67

A practical topic related to energy recycling is thermal integration. A useful tool for this integration is the pinch technology aiming to maximize the recycled energy in the process and minimize the amount of additional cooling/heating services needed by the process and thus decreasing the energy consumption costs. The advantages of this method

include the determination of maximum energy recycling in the entire process, and it proposes a specific method for this purpose. The main limitation of the pinch technology is that it only performs a thermal analysis of systems and cannot examine these systems' power or pivotal work. Therefore, in systems such as cooling and power production cycles that deal with power/pivotal work in addition to thermal energy, pinch energy should be developed. Since exergy analysis is an effective method for examining the power and pivotal work, by a proper integrating of exergy analysis and pinch technology, a practical and useful solution for the simultaneous examination of thermal energy and power consumed in systems can be achieved. This technique is referred to as the combined pinch and exergy analysis. Figure 4 displays a composite curve of multi-stream heat exchangers used in the hybrid unit. The closer the hot and cold diagrams of the exchangers to each other, the more efficient the heat is transferred, and the lower the energy consumption. On the other hand, the exchangers' heat transfer surface will increase, and hence, the exchangers' total volume and design complexity will increase.

Exergy composite curves, obtained by replacing the heat axis in the composite curve with the Carnot coefficient, are used as a key tool in the CPEA goal-setting stage. Figure 5 presents the specifications of the exergy composite curve of the multi-stream exchangers used in the integrated structure. Table 3 lists the operational specifications of the equipment used in the natural gas liquefaction hybrid unit by using the DMR compression refrigeration unit, Kalina power production cycle, and PV panels (Fig. 6). The simulation results show that the minimum temperature difference of the multi-stream exchangers is 3 °C.

Table 4 gives the specifications of the PV panels used in this plant. The simulation results of the PV system in PVsyst 6.8.1 are given below.

The variation of the monthly average horizontal global radiation is from 116.1 kWh m^{-2} in December to 208.1 kWh m^{-2} in May. The hottest month of the year with the monthly average temperature of 34.37 °C is June, while the coldest month of the year with the monthly average temperature of 20.61 °C is January. The average environment temperature in a sample year is 28.62 °C. Figure 7 presents the PR coefficient, array output energy, and the energy injected into the grid.

The difference in the monthly available solar injected energy of various systems over the year can be observed in the results. Maximum available solar energy was available in April (5.02 kWh/kWp/day), and the minimum available solar energy was observed in December (4.37 kWh/kWp/day). This may be due to the relatively higher global titled

plane solar irradiance in different months. The value of PR reaches its maximum (79%) in December and its minimum in May (79%). The annual mean value of PR is determined as 81%. System losses, collection losses, and useful energy production are given in Fig. 8.

Solar energy is absorbed by PV panels. Due to collection losses, this energy is reduced and is then distributed in the inverters. The distributed energy is injected into the grid as useful energy produced. Figure 9 displays the system, array, and inverter yield.

PV panels can produce electricity in a wide range of optical frequencies but cannot cover the entire solar spectrum. This is why a large amount of solar energy will be lost. Figure 10 illustrates different losses in the simulation of the present work.

The annual mean of module quality loss is 363.3 MWh. Maximum mismatch loss was 37.34 MWh in October, and minimum mismatch loss was 41.08 MWh in February. If the size and length of the cables are incorrectly chosen, this will directly affect the ohmic wiring loss; the mean annual ohmic wiring loss is 527.2 MWh.

Exergy analysis results

Exergy assessment is another method for examining the second law of thermodynamic to assess the quality of integrated structures. Exergy assessment is an engineering tool used for thermodynamic examination of the process and determining the maximum amount of useful work achievable from the specific amount of input energy. In exergy assessment, the reversibilities that increase the system's dissipated work are identified, and their degree of effect on the process efficiency is determined. The results of chemical, physical, and total exergy analysis of each flow used in the hybrid unit are given in Table 5.

Table 6 presents the values of the analysis of fuel exergy, product exergy, exergy destruction, and equipment efficiency in the developed hybrid unit.

The values of the exergy destruction ratio of the equipment in the developed hybrid unit are depicted in Fig. 11 via a pie chart.

The results of exergy assessment demonstrate that the highest exergy destruction ratio in the equipment belonged to PV panels and heat exchangers (86.29% and 6.51%, respectively). The values of the exergy destruction ratio of the heat exchangers in this work are given in Fig. 12.

Based on Fig. 12, the maximum exergy destruction ratio was in the HX7 heat exchanger (23.01%), whereas the minimum value belonged to the HX9 and HX10 heat exchangers (1.19%). Figure 13 presents the input exergy, output exergy,
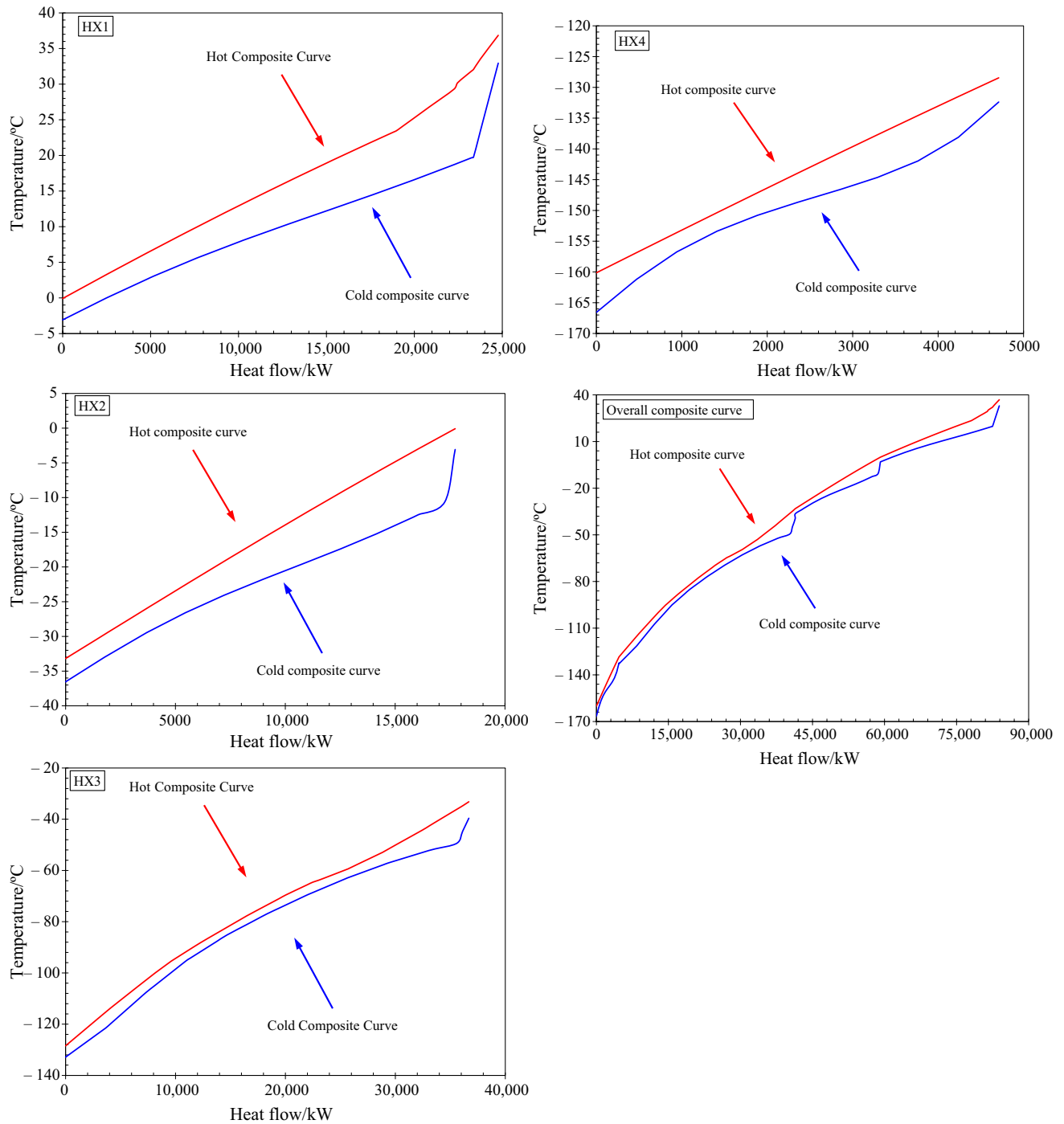
Fig. 4 Composite curve of multi-stream heat exchangers used for natural gas liquefaction

and exergy destruction of the equipment of the entire hybrid unit separately.

Economic analysis results

To perform the economic analysis of the present work, the feasibility study of the hybrid unit and the ACS method has been performed. Table 7 lists the price of the equipment used in the natural gas liquefaction hybrid unit. To update these prices, Marshal and Swift cost indices were used. Table 8 depicts the stages of the economic assessment of the developed hybrid unit for natural gas liquefaction. In calculating the economic analysis of the presented hybrid structures, the annual inflation rate, the bank's nominal interest rate, and the project's useful life have been assumed to be 17%, 20%, and 20 years, respectively.

Results The economic assessment of the hybrid unit revealed that the payback period, prime cost of product, annual net profit, and additive value equaled 2.061 years, 0.2500 US\$ kg^{-1} LNG, 5159 MMUS\$ Year^{-1}, and 0.1156 US\$ kg^{-1} LNG, respectively.

Validation of the integrated structure

For model validation, a comparison was performed with the PV system implemented by reference [41] for Tuticorin, India. Table 9 presents the validity of the PV model of this study compared to reference [41]. The comparison of results shows that the results of the present study are well compatible with those of reference [41]. Moreover, further comparisons of other cases are given in Table 9.

The results of validation of the cycle's COP and the specific power consumption of the natural gas liquefaction system using DMR compression refrigeration cycle compared to reference [2] are given in Fig. 14. After validation, the changes for applying industrial considerations were made to the cycle.

Based on the final price and the payback rate in the present study, and based on the results, the implementation of this integrated structure is feasible and justifiable. The final price in this study is 0.25 US\$ kg^{-1} LNG. The validation of the final price of the liquefied natural gas with similar structures in research and industry [4, 6, 42] is shown in Fig. 15.

Sensitivity analysis of the developed integrated structure

To evaluate the developed integrated structure in different economic conditions, sensitivity analysis was performed on the economical parameters. The parameters of the payback period, the prime cost of product, and investment cost are effective parameters for examining a suitable hybrid unit for natural gas liquefaction. The results of the economic analysis revealed that this structure is economically justified for implementation. Figure 16 displays the effects of changes in the payback period and the annual net profit compared to changes in the price of liquefied natural gas. The findings of the economic sensitivity assessment demonstrate that, by increasing the price of liquefied natural gas from 3 to 11 US\$/MMBTU in different regions of the world, the payback period is reduced from 3.07 to 1.72 years and the annual net profit is increased from 418.4 to 747.4 MMUS\$/Year.

Figure 17 illustrates the effects of changes in the prime cost of the product and LCOP compared to the investment price. The findings of economical sensitivity analysis revealed that, by increasing the primary investment cost from 643 to 3730 MMUS\$, the prime cost of product was

Fig. 5 Exergy composite curve
of multi-stream heat exchangers
used for natural gas liquefaction
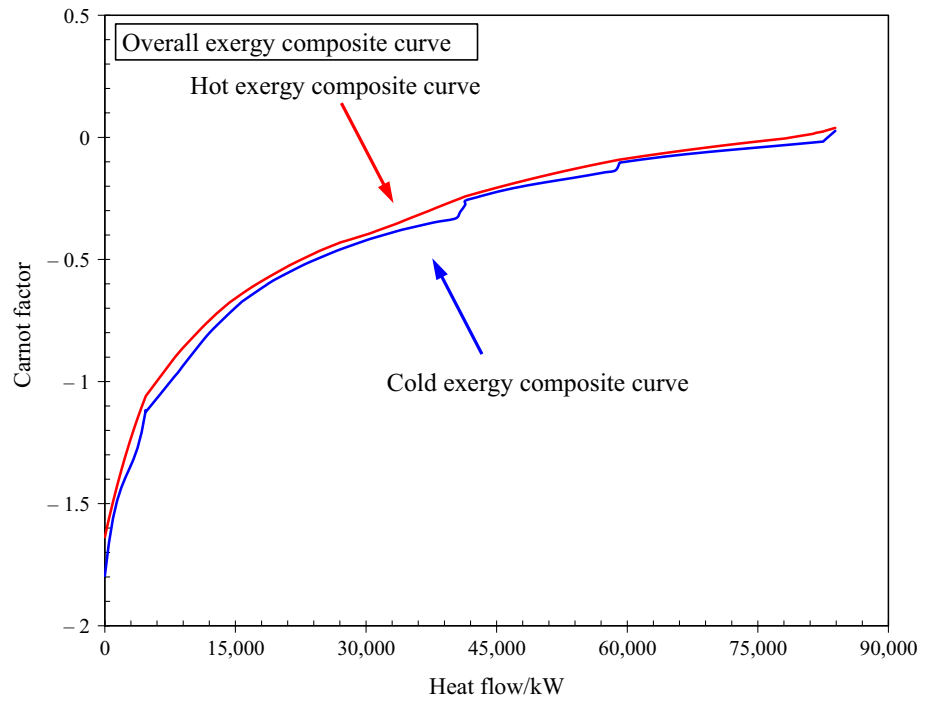
Fig. 6 Monthly average ambient
temperature and solar irra-
diation for a sample year in
Chabahar
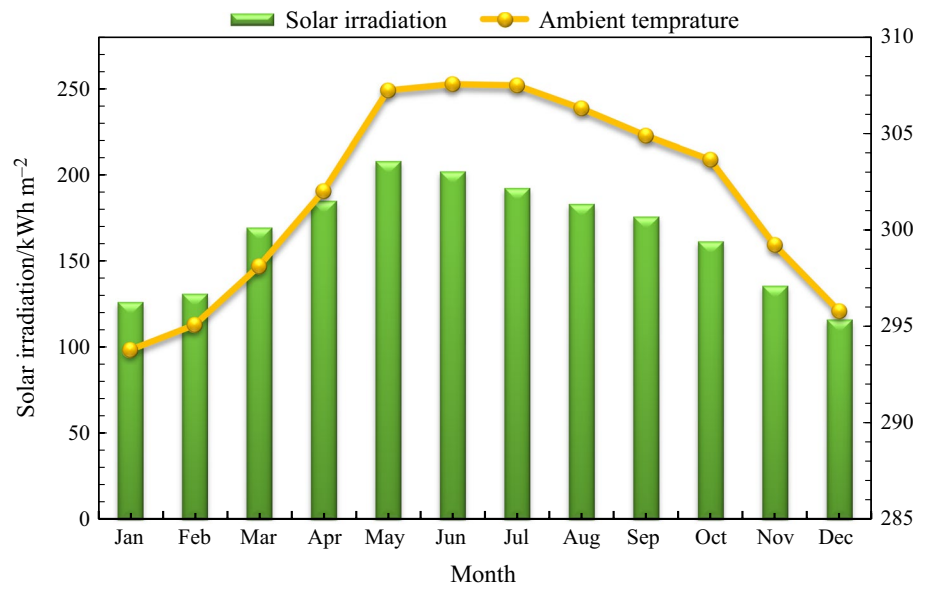
Table 3 Operational specifications of the equipment used in the integrated structure

Pump	Adiabatic efficiency/%	Power/kW	ΔP/kPa	P ratio/−
P1	80.00	17.63	220.0	1.500

Compressor	Adiabatic efficiency/%	Power/kW	ΔP/kPa	P ratio/−
C1	80.00	6175	1160	2.526
C2	75.00	2691	480.0	2.714
C3	80.00	13,265	1747	6.770
C4	80.00	2887	1106	1.540
C5	80.00	2896	1704	1.540

Turbine	Isentropic efficiency/%	Power/kW	ΔP/kPa	P ratio/−
T1	90.00	17.25	190.0	0.703

Heat exchanger	Min. approach/℃	LMTD/℃	Duty/kW	Cold pinch temp./℃
HX1	3.000	5.253	24,767	−3.080
HX2	3.000	5.202	17,731	−3.080
HX3	3.000	4.551	36,686	−85.20
HX4	3.012	4.663	4709	−153.3
HX5	24.15	25.00	2056	6.844
HX6	1.588	4.015	9038	78.00
HX7	5.477	10.50	38,110	78.44
HX8	8.464	15.27	5145	53.78
HX9	25.66	36.01	764.6	49.00
HX10	0.800	9.360	52,643	6.000

Table 4 Specifications of the PV used in this study

Specification			
Electrical performance under standard test conditions (STC)		Electrical performance at 800 W m^{-2}, NOCT, AM 1.5	
Maximum power (P_{max})	400 W ($\pm$ %3)	Maximum power (P_{max})	322.2 W
Maximum power voltage (V_{mpp})	40.6 V	Maximum power voltage (Vmpp)	40.4 V
Maximum power current (I_{mpp})	9.86 A	Maximum power current (I_{mpp})	7.98 A
Open circuit voltage (V_{oc})	49.3 V	Open circuit voltage (V_{oc})	48.9 V
Short circuit voltage (I_{sc})	10.47 A	Short circuit voltage (I_{sc})	8.38 A
Maximum system voltage	1000 V		
Temperature coefficient of V_{oc}	−138 mV ℃$^{-1}$	Module characteristics	
Temperature coefficient of I_{sc}	3.1 mA ℃$^{-1}$	Length × Width × depth/mm	2024 × 1024 × 40
Cell		Mass (kg)	21.7
Number per module	66,300		

[a]STC: irradiance 1000 W m^{-2}, AM 1.5 spectrum, module temperature 25 ℃

Nominal operating cell temperature (NOCT): 25 ℃

Fig. 7 Monthly array energy production and the energy injected into the grid and PR
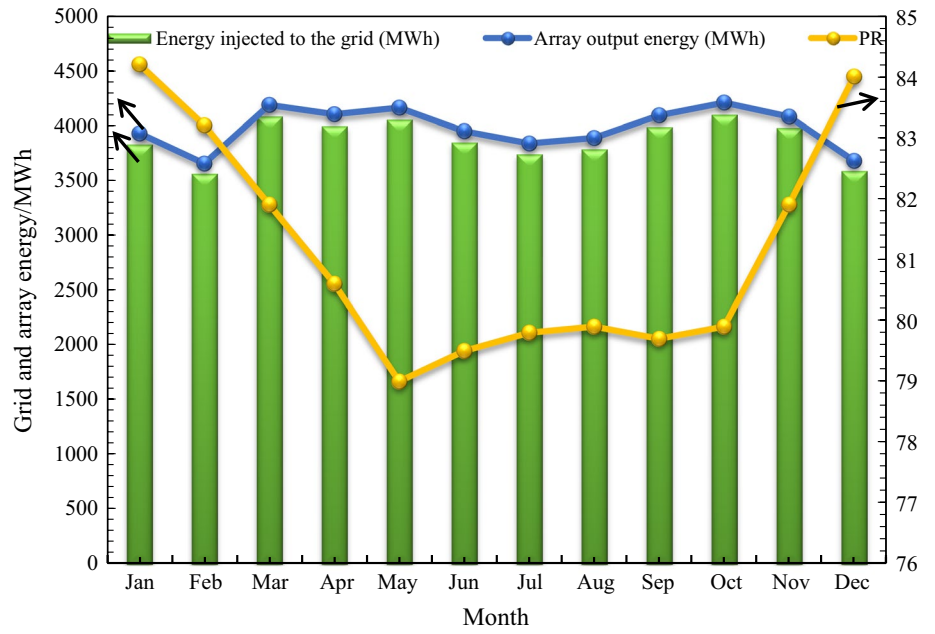
Fig. 8 Normalized energy per month
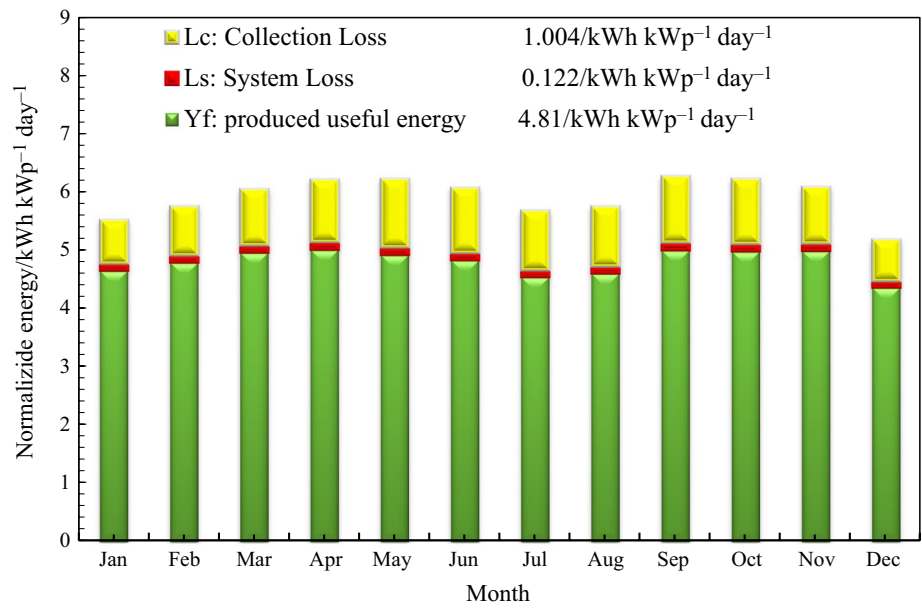
Fig. 9 Inverter, system, and array yield in a sample year
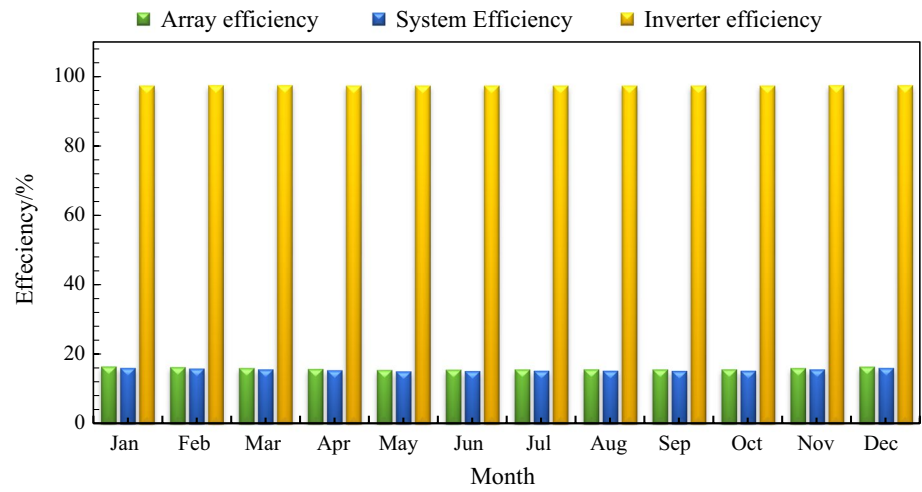
Fig. 10 System loss diagram over the whole year
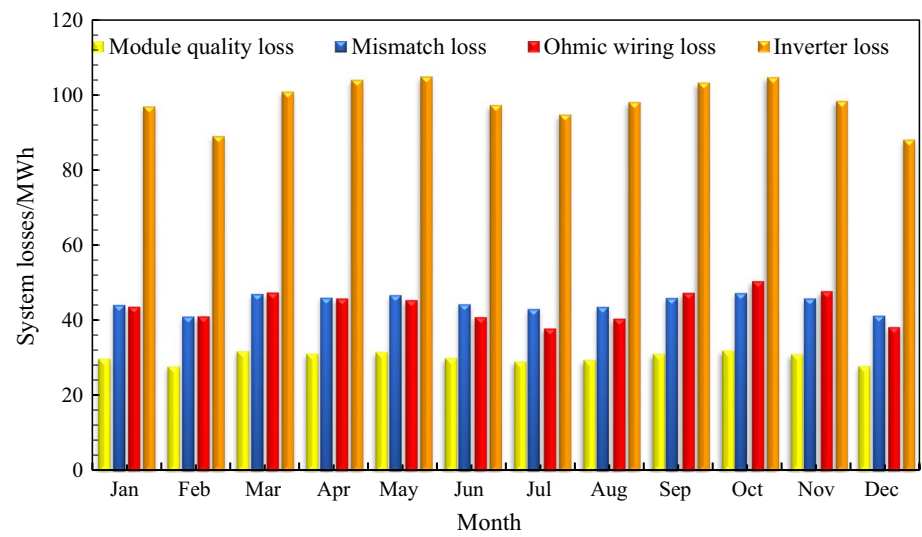
Table 5 Information on the physical, chemical, and total exergy analysis of the flows used in the integrated structure

Stream	Physical exergy/kW	Chemical exergy/kW	Total exergy/kW	Stream	Physical exergy/kW	Chemical exergy/kW	Total exergy/kW
1	16,055.60	4,752,119.54	4,768,175.14	31	18,658.04	1,664,336.53	1,682,994.57
2	13,121.80	4,752,119.54	4,765,241.34	32	18,761.94	1,664,336.53	1,683,098.47
3	13,343.20	4,752,119.54	4,765,462.73	33	19,353.66	1,664,336.53	1,683,690.20
4	5337.28	1,900,847.81	1,906,185.09	34	28,399.74	1,664,336.53	1,692,736.27
5	5840.88	1,900,847.81	1,906,688.70	35	32,876.18	1,664,336.53	1,697,212.72
6	5705.22	1,900,847.81	1,906,553.03	36	31,626.79	1,664,336.53	1,695,963.33
8	4392.44	1,900,847.81	1,905,240.25	38	470.84	68,566.68	69,037.53
9	10,920.05	4,752,119.54	4,763,039.59	39	8104.38	719,778.99	727,883.38
10	8005.92	2,851,271.72	2,859,277.64	40	8104.38	719,778.99	727,883.38
11	7868.12	2,851,271.72	2,859,139.84	41	1300.97	115,543.78	116,844.75
12	6535.98	2,851,271.72	2,857,807.70	42	902.81	80,181.61	81,084.42
13	22,690.83	3,161,458.72	3,184,149.55	43	5760.66	511,624.62	517,385.28
14	22,343.67	3,161,458.72	3,183,802.39	44	139.94	12,428.99	12,568.94
15	22,808.45	3,161,458.72	3,184,267.17	45	1558.01	115,543.78	117,101.79
16	24,589.83	3,161,458.72	3,186,048.55	46	5681.80	511,624.62	517,306.41
19	12,620.14	601,648.56	614,268.70	49	9456.99	719,778.99	729,235.98
20	12,244.08	601,648.56	613,892.64	50	171.98	61,920.27	62,092.25
21	5576.40	601,648.56	607,224.96	51	81.22	61,920.27	62,001.49
22	29,220.94	3,161,458.72	3,190,679.67	52	79.21	61,920.27	61,999.47
23	7700.13	3,161,458.72	3,169,158.85	53	9210.93	657,858.73	667,069.66
24	18,662.13	3,161,458.72	3,180,120.85	54	9210.91	657,858.73	667,069.64
25	18,054.80	3,161,458.72	3,179,513.52	55	7314.95	657,858.73	665,173.68
26	20,397.12	3,161,458.72	3,181,855.84	56	7392.42	719,778.99	727,171.41
27	20,312.29	3,161,458.72	3,181,771.01	57	1755.25	444,584.30	446,339.55
28	16,916.90	2,560,509.89	2,577,426.80	58	−0.02	444,584.30	444,584.28
29	23,938.60	2,560,509.89	2,584,448.49	59	8089.29	719,778.99	727,868.29
30	22,985.70	2,560,509.89	2,583,495.59	60	6920.70	511,624.62	518,545.32

Table 6 Information on the analysis of fuel exergy, product exergy, exergy destruction, and equipment efficiency

Equipment	Exergy fuel rate/kW	Exergy product rate/kW	Exergy destruction rate/kW	Efficiency
HX1	12,491,178.14	12,490,636.08	542.07	0.9002
HX2	8,680,695.49	8,679,617.92	1077.57	0.9726
HX3	8,060,418.42	8,058,864.76	1553.65	0.9577
HX4	2,919,150.06	2,918,706.38	443.68	0.9058
HX5	3,699,241.12	3,699,077.43	163.69	0.9204
HX6	3,296,965.60	3,296,615.31	350.29	0.9612
HX7	5,285,481.55	5,283,786.66	1694.90	0.9555
HX8	3,265,233.97	3,264,929.14	304.83	0.9408
HX9	74,661.19	74,573.21	87.98	0.8849
HX10	74,661.19	74,573.21	87.98	0.8849
HX11	1,173,510.96	1,172,452.57	1058.40	0.9799
T1	667,069.64	666,898.76	170.88	0.9099
C1	4,769,214.82	4,768,175.14	1039.68	0.8316
C2	1,905,881.99	1,905,240.25	641.74	0.7616
C3	3,182,424.46	3,180,120.85	2303.61	0.8263
C4	3,182,400.68	3,181,855.84	544.83	0.8113
C5	3,184,667.23	3,184,149.55	517.67	0.8213
P1	727,885.91	727,883.38	2.53	0.8562
S1	1,695,963.33	1,695,963.33	0.00	1.0000
S2	3,186,048.55	3,186,048.55	0.00	1.0000
S3	729,235.98	729,161.91	74.07	1.0000
V1	2,859,277.64	2,859,139.84	137.80	0.7621
V2	614,268.70	613,892.64	376.07	0.6752
V3	1,697,212.72	1,695,963.33	1249.39	0.7324
V4	2,584,448.49	2,583,495.59	952.90	0.6722
V5	1,906,688.70	1,906,553.03	135.67	0.8628
V6	727,883.38	727,883.38	0.00	0.8421
V7	667,069.66	667,069.64	0.02	0.7721
V8	62,001.49	61,999.47	2.01	0.5847
PV	125,878.66	28,206.00	97,672.66	0.2241
Cycle	172,470.04	59,283.88	113,186.17	0.4277
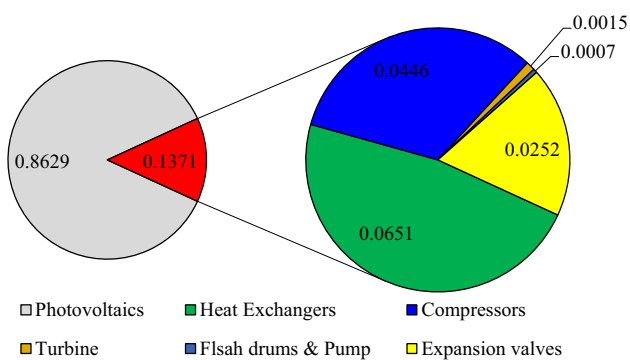
Fig. 11 Pie chart of the exergy destruction ratio of equipment in the integrated structure

increased from 0.1728 to 0.5434 US\$ kg^{-1} LNG, and the LCOP was raised from 0.2107 to 0.7807 US\$ kg^{-1} LNG. Figure 18 illustrates the effects of changes in the annual net profit of the product and payback period compared to the investment price. Evidently, for the equipment price of 2100 MMUS\$ and less, the payback period is < 4 years. Note that a payback period of < 4 years in natural gas liquefaction is economically justifiable.

Fig. 12 Pie chart of the exergy destruction ratio of the heat exchangers used in the developed integrated structure

HE1
HE2
HE3
HE4
HE5
HE6
HE7
HE8
HE9
HE10
HE11
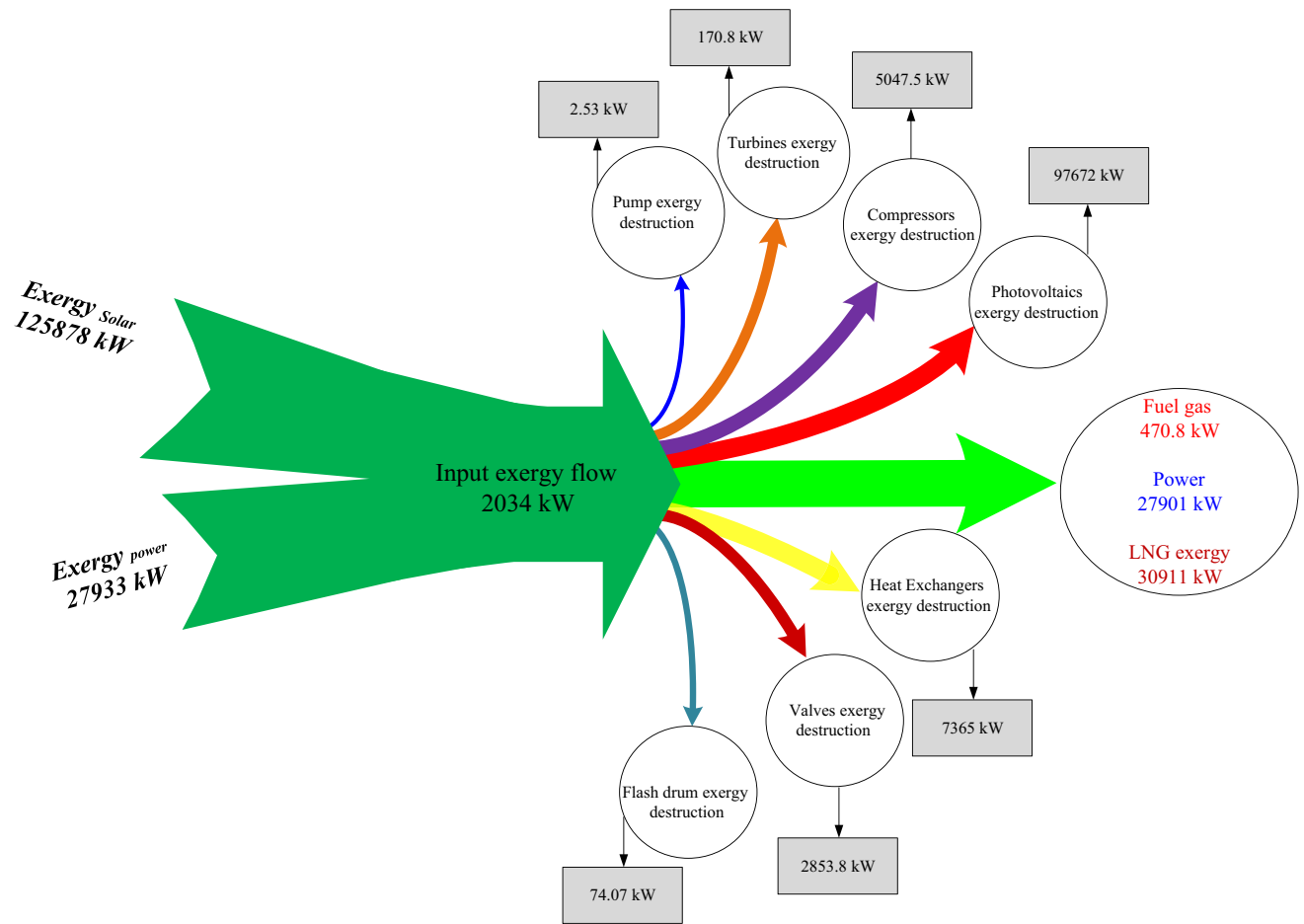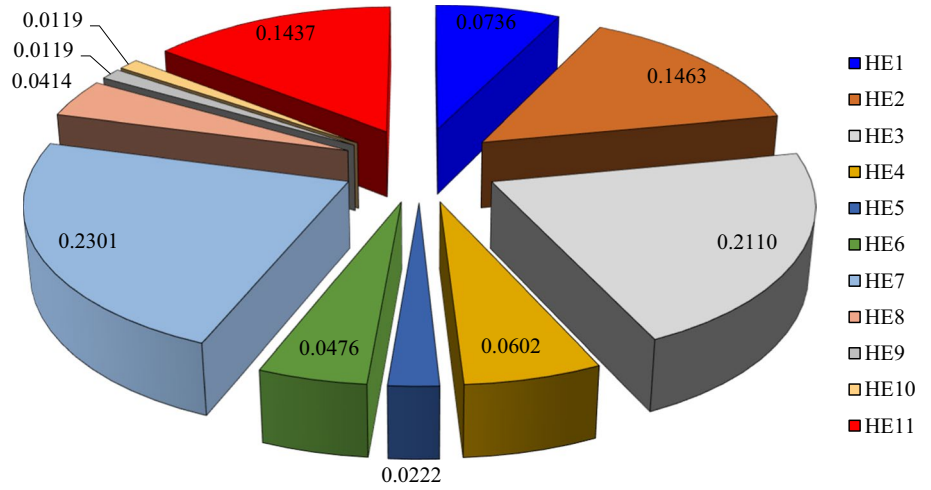
Fig. 13 Value of input exergy, output exergy, and exergy destruction of the entire developed integrated structure

Table 7 The prices of the equipment used in the natural gas liquefaction integrated structure [31, 38]

Component	Purchased equipment cost functions
Compressor	$C_{\text{Com}} = \left(\frac{39.5 \times \dot{m}}{\eta_{\text{C}}}\right)\left(\frac{p_{\text{discharge}}}{p_{\text{suction}}}\right)\ln\left(\frac{p_{\text{discharge}}}{p_{\text{suction}}}\right)$ $C_{\text{Com}} = $ Cost of compressor (k$)
Photovoltaic	$C_{\text{PV}} = 840$ \$ m^{-2} (PV array cost) $C_{\text{Battery cost}} = 220$ \$/kWh, $C_{\text{Inverter cost}} = 750$ \$/kWh $C_{\text{Diesel genset cost}} = 550$ \$/kWh
Heat exchanger	$C_{\text{E}} = a(V)^{\text{b}} + c$ $C_{\text{E}} = $ Cost of heat exchanger (\$)
Condenser	$C_{\text{C}} = 516.621 \times A_{\text{Condenser}} + 268.45$
Pump	$C_p = \dfrac{705.48 \times W_{\text{Pump}}^{0.71}\left(1 + \dfrac{0.2}{1-\eta_{\text{Pump}}}\right)}{}$
General heat exchanger	$C_{HX} = 8500 + 409 \times A_{\text{HX}}^{0.85}$
Flash Drum	$C_{\text{D}} = f_{\text{m}}C_b + C_a$ $C_{\text{D}} = $ Cost of drum (\$) $C_b = 1.218\exp[9.1 - 0.2889(\ln W) + 0.04576(\ln W)^2]$, $5000 < W < 226{,}000$ lb shell mass $C_a = 300 D^{0.7396} L^{0.7066},\ 6 < D < 10,\ 12 < L < 20$ ft $f_{\text{m}} = $ Material Factor

Table 8 Stages of the economic analysis of the developed integrated structure for natural gas liquefaction [40, 43, 44]

Definition	Parameter
Annualized operating cost Operating flow cost	OFC = (*Labor Cost + Fuel Cost + Insurance Cost + Utility*) *Number of labor = 50, Labor Cost = 400 US$ per Month* *Fuel Cost (Natural Gas Price) = 2 (US$ per Million Btu)* *Insurance Cost = 0.02 of Capital Cost*
Net present value	*NPV = ACS/ CRF(i,Yproj)*
Levelized cost of product Total product in one Year (kg LNG)	*LCOP = ACS/ Total Product in one Year*
Prime cost	*VOP = Volume of Product, PC = OFC/VOP*
Summary of product cost	*COP = Cost Of Product, SOPC = VOP. COP* *COP = 8 (US$ per Million Btu)*
Annual benefit	*AB = SOPC- OFC*
Net annual benefit	*NAB = AB.(1-Tax percent), Tax = 0.1(AB)*
Period of return	*POR = Ccap/NAB*
Rate of return	*ROR = NAB/ Ccap*
Additive value	*AV = COP-PC*

Table 9 Model validation for the PV system compared to the reference [41]

Model validation for PV system			
Items	Present study	Ref. (Kandasamy et al., 2013)	Error/%
Ambient temperature/ºC	27.30	26.86	1.638
EArray/MWh	1664	1565	6.325
E_grid/MWh	1618	1522	6.307
EffArrR/%	12.70	11.79	7.718
EffSysR/%	12.35	11.46	7.766

Fig. 14 Results of the validation of operational parameters of the natural gas liquefaction cycle with the reference [2]
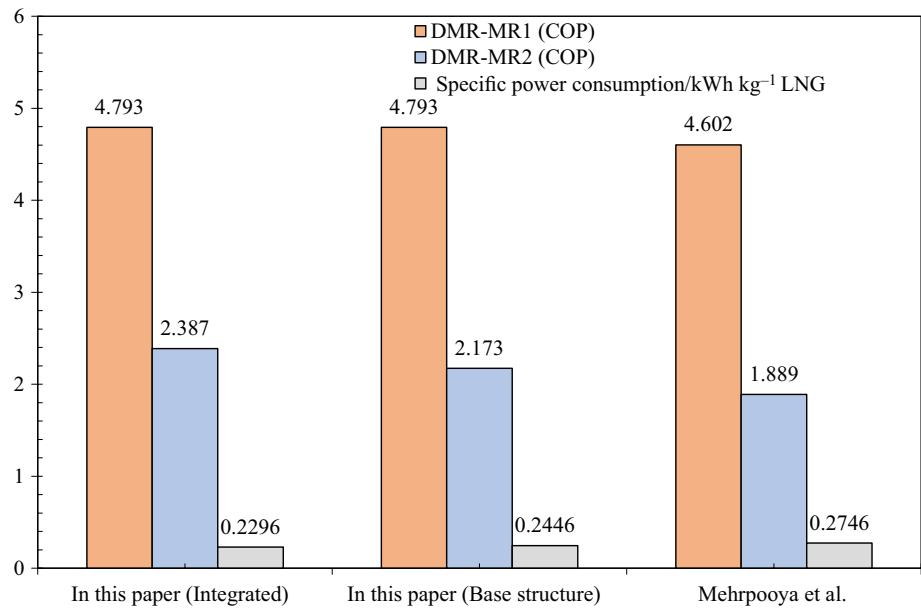
Fig. 15 Results of the validation of the liquefied natural gas in the developed integrated structure with the references [4, 6, 42]
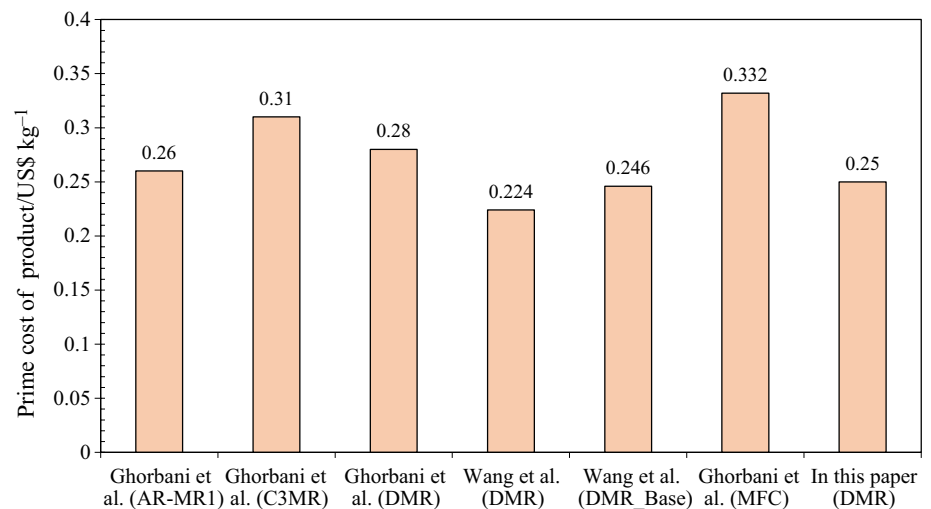
Fig. 16 Changes in the payback period and net annual benefit compared to the price of the produced liquefied natural gas
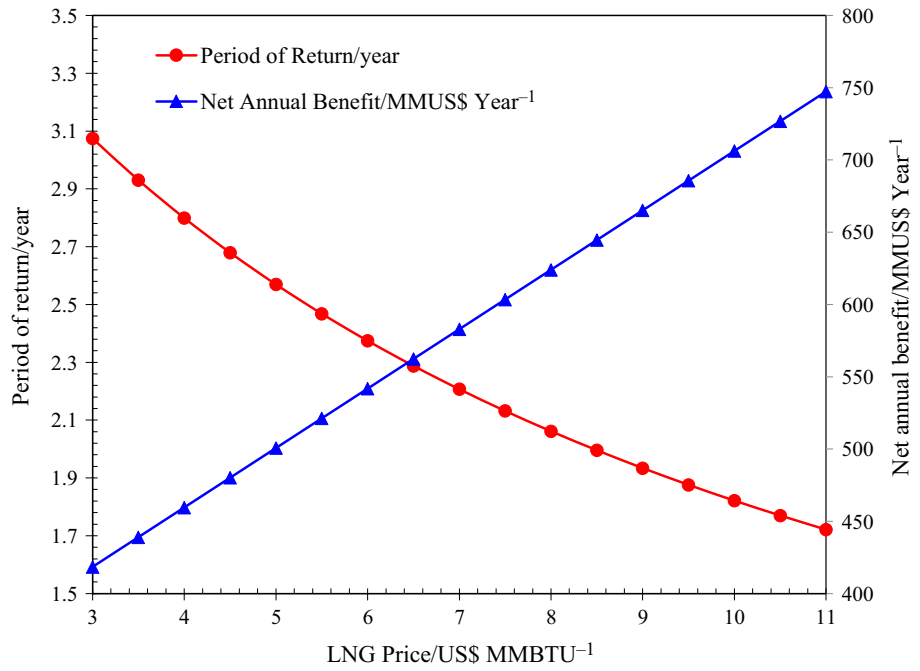
Fig. 17 Changes in the prime cost of the product and LCOP compared to the primary investment price
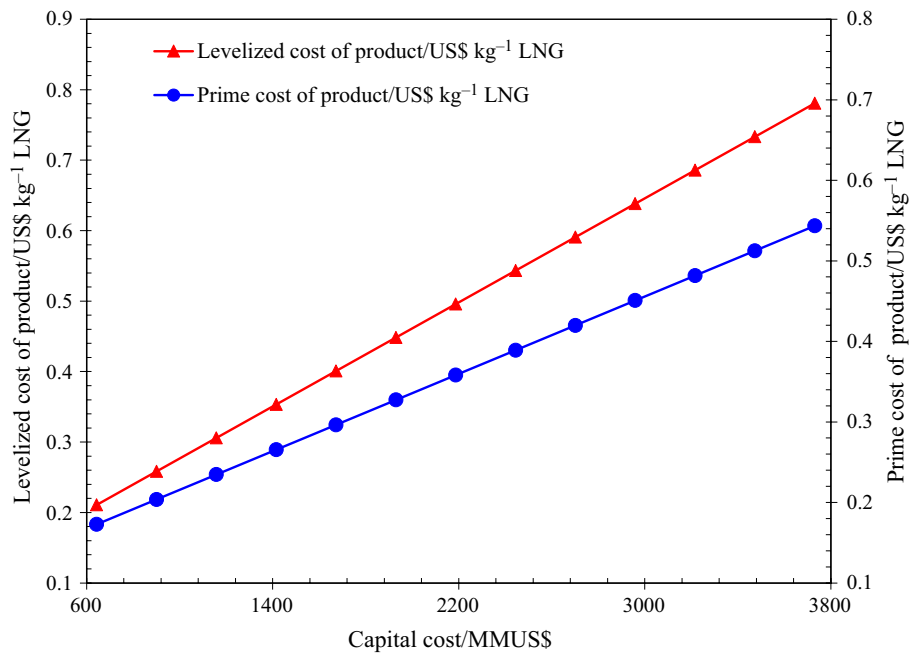
Fig. 18 Changes in the net annual benefit and the payback period compared to the investment cost
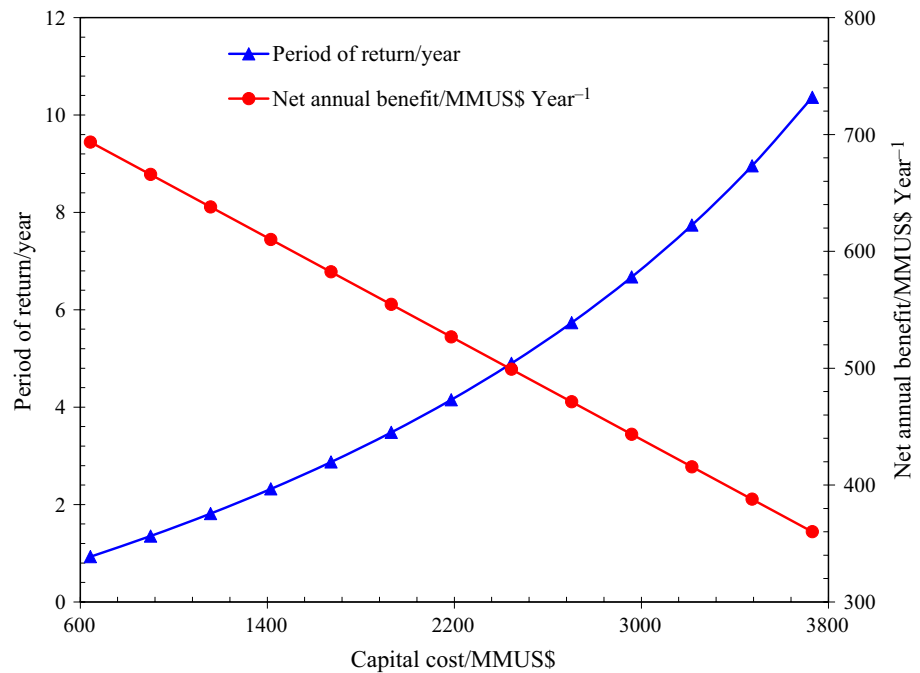
Conclusions

One of the problems of renewable systems is energy storage because all these systems work in a specific period, and the energy production in them is not permanent and continuous. Moreover, to transfer natural gas and prevent an outage on cold days of the year due to a pressure drop in the grid, the manufacture of LNG demand response devices with lower energy consumption has received the attention of many researchers. In this study, a solar energy and natural gas storage method was developed by using a natural gas liquefaction system, DMR compression refrigeration cycle, Kalina power production cycle, and photovoltaic (PV) solar panels compatible with the climate of Chabahar coastal city in Southern Iran. The results of thermodynamic, exergy, and economic analysis of the developed integrated structure are reported below:

1. By consuming 6771 kmol/h natural gas and 26.17 MW of power provided by solar panels, this integrated structure produces 6301 kmol/h liquefied natural gas. The COP of the pre-cooling DMR compression refrigeration cycle, liquefaction cycle, and the entire hybrid unit equals 4.793, 2.387, and 3.201, respectively. In this hybrid unit, 54.35 MW of dissipated heat is used in the Kalina power production cycle which produces 1743 kW power. To provide cooling in the condenser of the Kalina cycle, layers of oceanic water were used. The specific energy consumption and thermal yield of the Kalina cycle in the integrated structure equaled 0.2293 and 3.206%, respectively.

2. The exergy assessment of the hybrid unit showed that the maximum exergy destruction of the integrated structure in PV panels is 86.29% of the entire integrated structure (97.67 MW), and the rest belongs to the other facilities. From among the heat exchangers, the maximum exergy destruction belonged to the HX2 exchanger (14.63%) and the minimum value belonged to the HX9 exchanger (1.194%). The exergy efficiency and the exergy destruction of the entire integrated structure equaled 113.1 MW and 42.77%, respectively.

3. The ACS method was adopted to evaluate the integrated structure. The results of the economic analysis revealed that the parameters of payback period, final product price, and primary investment price are effective parameters for selecting a suitable integrated structure in the natural gas supercooling integrated systems. Based on the results of economic analysis, the hybrid structure is economically justified for implementation.

4. The payback period, prime cost of product, and the investment price were calculated as 2.061 years, 0.2500 US$ kg^{-1} LNG, and 1286 MMUS$. The findings of the sensitivity analysis showed that, by increasing the price of liquefied natural gas from 3 to 11 US$/MMBTU, the payback period is reduced from 3.07 to 1.72 years and the annual net profit is increased from 418.4 to 747.4 MMUS$/Year.

5. The future directions of research could include advanced exergy analysis, advanced exergoeconomic analysis, and dynamic analysis of the present integrated structure. Moreover, other new energies such as wind turbines can

be used in regions with good wind power to provide the power of the natural gas liquefaction cycle.

Declarations

References

1. Ghorbani B, Hamedi M-H, Amidpour M. Development and optimization of an integrated process configuration for natural gas liquefaction (LNG) and natural gas liquids (NGL) recovery with a nitrogen rejection unit (NRU). Journal of Natural Gas Science and Engineering. 2016;34:590–603.

2. Vatani A, Mehrpooya M, Palizdar A. Energy and exergy analyses of five conventional liquefied natural gas processes. Int J Energy Res. 2014;38(14):1843–63.

3. Vatani A, Mehrpooya M, Palizdar A. Advanced exergetic analysis of five natural gas liquefaction processes. Energy Convers Manage. 2014;78:720–37.

4. Ghorbani B, Hamedi M-H, Amidpour M, Shirmohammadi R. Implementing absorption refrigeration cycle in lieu of DMR and C3MR cycles in the integrated NGL, LNG and NRU unit. Int J Refrig. 2017;77:20–38. https://doi.org/10.1016/j.ijrefrig.2017.02.030.

5. Ghorbani B, Shirmohammadi R, Mehrpooya M. A novel energy efficient LNG/NGL recovery process using absorption and mixed refrigerant refrigeration cycles—economic and exergy analyses. Appl Therm Eng. 2018;132:283–95.

6. Wang M, Khalilpour R, Abbas A. Thermodynamic and economic optimization of LNG mixed refrigerant processes. Energy Convers Manage. 2014;88:947–61.

7. Qyyum MA, He T, Qadeer K, Mao N, Lee S, Lee M. Dual-effect single-mixed refrigeration cycle: an innovative alternative process for energy-efficient and cost-effective natural gas liquefaction. Appl Energy. 2020;268:115022.

8. Khan MS, Chaniago YD, Getu M, Lee M. Energy saving opportunities in integrated NGL/LNG schemes exploiting: thermal-coupling common-utilities and process knowledge. Chem Eng Process. 2014;82:54–64.

9. Mehrpooya M, Hossieni M, Vatani A. Novel LNG-based integrated process configuration alternatives for coproduction of LNG and NGL. Ind Eng Chem Res. 2014;53(45):17705–21.

10. Shazed AR, Ashraf HM, Katebah MA, Bouabidi Z, Al-musleh EI. Overcoming the energy and environmental issues of LNG plants by using solid oxide fuel cells. Energy. 2021;218:119510.

11. Morosuk T, Tesch S, Hiemann A, Tsatsaronis G, Omar NB. Evaluation of the PRICO liquefaction process using exergy-based methods. J Nat Gas Sci Eng. 2015;27:23–31.

12. Khan MS, Karimi I, Lee M. Evolution and optimization of the dual mixed refrigerant process of natural gas liquefaction. Appl Therm Eng. 2016;96:320–9.

13. Husnil YA, Lee M. Synthesis of an optimizing control structure for dual mixed refrigerant process. J Chem Eng Jpn. 2014;47(8):678–86.

14. Sun H, Shu D, Jiang Z. Simulation study of the dynamic performance of a MRC plant with refrigerant charged or leaked. Cryogenics. 2012;52(1):8–12.

15. Narasimhan NL, Venkatarathnam G. A method for estimating the composition of the mixture to be charged to get the desired composition in circulation in a single stage JT refrigerator operating with mixtures. Cryogenics. 2010;50(2):93–101.

16. Colmenares T, Seider W. Synthesis of cascade refrigeration systems integrated with chemical processes. Comput Chem Eng. 1989;13(3):247–58.

17. Vaidyaraman S, Maranas CD. Optimal synthesis of refrigeration cycles and selection of refrigerants. AIChE J. 1999;45(5):997–1017.

18. Aghazadeh Dokandari D, Seyyed Mahmoudi SM, Setayesh HA. Thermodynamic analysis and optimization of a novel ejector-cascade refrigeration cycle. Modares Mech Eng. 2014;14(7):85–93.

19. Nawaz A, Qyyum MA, Qadeer K, Khan MS, Ahmad A, Lee S, et al. Optimization of mixed fluid cascade LNG process using a multivariate Coggins step-up approach: overall compression power reduction and exergy loss analysis. Int J Refrig. 2019;104:189–200.

20. Pereira C, Handaya A, Sutrasno K. Thermodynamic analysis for liquefaction of natural gas using the C3-MR refrigeration process. Int J Chem Eng Appl. 2014;5(1):17.

21. Sahoo U, Kumar R, Singh S, Tripathi A. Energy, exergy, economic analysis and optimization of polygeneration hybrid solar-biomass system. Appl Therm Eng. 2018;145:685–92.

22. Ebrahimi A, Ghorbani B, Skandarzadeh F, Ziabasharhagh M. Introducing a novel liquid air cryogenic energy storage system using phase change material, solar parabolic trough collectors, and Kalina power cycle (process integration, pinch, and exergy analyses). Energy Convers Manag. 2020;2020:113653.

23. Gordon JM, Moses G, Katz EA. Boosting silicon photovoltaic efficiency from regasification of liquefied natural gas. Energy. 2020;214:118907.

24. Sharadga H, Dawahdeh A, Al-Nimr MdA. A hybrid PV/T and Kalina cycle for power generation. Int J Energy Res. 2018;42(15):4817–29.

25. Ghorbani B, Zendehboudi S, Moradi M. Development of an integrated structure of hydrogen and oxygen liquefaction cycle using wind turbines, Kalina power generation cycle, and electrolyzer. Energy. 2020;2020:119653.

26. Einemann M, Petersen T. Design and Optimization of a Kalina Cycle. 2015.

27. Naeimi A, Bidi M, Ahmadi MH, Kumar R, Sadeghzadeh M, Nazari MA. Design and exergy analysis of waste heat recovery system and gas engine for power generation in Tehran cement factory. Therm Sci Eng Prog. 2019;9:299–307.

28. Ghazvini M, Dehghani Madvar M, Ahmadi MH, Rezaei MH, El Haj AM, Nabipour N, et al. Technological assessment and modeling of energy-related CO₂ emissions for the G8 countries by using hybrid IWO algorithm based on SVM. Energy Sci Eng. 2020;8(4):1285–308.

29. Kumar R, Ahmadi MH, Rajak DK. The economic viability of a thermal power plant: a case study. J Therm Anal Calorim. 2020;20:1–7.

30. Ahmadi M, Sadaghiani M, Pourfayaz F, Ghazvini M, Mahian O, Mehrpooya M, et al. Energy and exergy analyses of a solid oxide fuel cell-gas turbine-organic Rankine cycle power plant with liquefied natural gas as heat sink. Entropy. 2018;2020(7):484.

31. Ghorbani B, Javadi Z, Zendehboudi S, Amidpour M. Energy, exergy, and economic analyses of a new integrated system for generation of power and liquid fuels using liquefied natural gas regasification and solar collectors. Energy Convers Manage. 2020;219:112915.

32. Okello D, Van Dyk E, Vorster F. Analysis of measured and simulated performance data of a 3.2 kWp grid-connected PV system in Port Elizabeth, South Africa. Energy Convers Manag. 2015;100:10–5.

33. Ghorbani B, Ebrahimi A, Moradi M, Ziabasharhagh M. Continuous production of cryogenic energy at low-temperature using two-stage ejector cooling system, Kalina power cycle, cold energy storage unit, and photovoltaic system. Energy Convers Manage. 2021;227:113541.

34. Shukla A, Khare M, Shukla K. Experimental exergetic performance evaluation of solar PV module. Int J Sci Res Publ. 2015;5(1):1–9.

35. Nouri M, Miansari M, Ghorbani B. Exergy and economic analyses of a novel hybrid structure for simultaneous production of liquid hydrogen and carbon dioxide using photovoltaic and electrolyzer systems. J Clean Prod. 2020;2020:120862.

36. Ghorbani B, Ebrahimi A, Moradi M, Ziabasharhagh M. Energy, exergy and sensitivity analyses of a novel hybrid structure for generation of bio-liquefied natural gas, desalinated water and power using solar photovoltaic and geothermal source. Energy Convers Manage. 2020;222:113215.

37. Ahmadi MH, Banihashem SA, Ghazvini M, Sadeghzadeh M. Thermo-economic and exergy assessment and optimization of performance of a hydrogen production system by using geothermal energy. Energy Environ. 2018;29(8):1373–92.

38. Ghorbani B, Miansari M, Zendehboudi S, Hamedi M-H. Exergetic and economic evaluation of carbon dioxide liquefaction process in a hybridized system of water desalination, power generation, and liquefied natural gas regasification. Energy Convers Manage. 2020;205:112374.

39. Ebrahimi A, Ziabasharhagh M. Optimal design and integration of a cryogenic Air Separation Unit (ASU) with Liquefied Natural Gas (LNG) as heat sink, thermodynamic and economic analyses. Energy. 2017;126:868–85.

40. Sameti M, Haghighat F. Optimization of 4th generation distributed district heating system: design and planning of combined heat and power. Renewable Energy. 2019;130:371–87.

41. Kandasamy C, Prabu P, Niruba K, editors. Solar potential assessment using PVSYST software. 2013 International Conference on Green Computing, Communication and Conservation of Energy (ICGCE); 2013: IEEE.

42. Ghorbani B, Shirmohammadi R, Mehrpooya M, Hamedi M-H. Structural, operational and economic optimization of cryogenic natural gas plant using NSGAII two-objective genetic algorithm. Energy. 2018;159:410–28.

43. Bilal BO, Sambou V, Ndiaye P, Kébé C, Ndongo M, editors. Multi-objective design of PV-wind-batteries hybrid systems by minimizing the annualized cost system and the loss of power supply probability (LPSP). 2013 IEEE International Conference on Industrial Technology (ICIT); 2013: IEEE.

44. Yang H, Zhou W, Lu L, Fang Z. Optimal sizing method for stand-alone hybrid solar–wind system with LPSP technology by using genetic algorithm. Sol Energy. 2008;82(4):354–67.

Publisher's Note Springer Nature remains neutral with regard to jurisdictional claims in published maps and institutional affiliations.